Thermohaline Oscillations in the LSG OGCM: Propagating Anomalies and Sensitivity to Parameterizations

TIMOTHY J. OSBORN

Climatic Research Unit, University of East Anglia, Norwich, United Kingdom

(Manuscript received 2 December 1996, in final form 14 April 1997)

ABSTRACT

New experiments are reported that extend previous studies of the internally generated variability found when the Hamburg LSG Ocean General Circulation Model is integrated under mixed boundary conditions. All model integrations have stochastic forcing added to the freshwater flux to excite the variability. It is demonstrated that the salinity anomalies that propagate around the meridional circulation of the Atlantic Ocean are merely signals emitted from the source of the variability in the Southern Ocean; they do not play an active role in its generation. It is the Southern Ocean flip–flop oscillator, as suggested by a previous study, that is the driving mechanism of the 320-yr period oscillations. A second mode of propagation is identified that may be related to the periodicity of the oscillations: westward propagation of upper-ocean salinity anomalies around the coast of Antarctica. It is shown that this mode is driven by the same density-upwelling wave motion as reported elsewhere in the literature.

The sensitivity of the simulated variability to changes in some of the model's numerical and physical algorithms is investigated. The computationally expensive step of retriangularizing the matrix equation for the barotropic velocity can be done very infrequently without affecting the characteristics of the variability. Changing to a convective overturn parameterization that leaves fewer residual instabilities has a small effect on the variability, while changing to one that mixes, rather than interchanges, statically unstable water masses can reduce the magnitude of the variability by up to 70%. The latter change, however, is attributed entirely to the different freshwater flux forcing that the new parameterization implies. Using a more realistic haline and thermal coupling between sea ice and the ocean also leads to greatly reduced internal variability on the 320-yr timescale. Again, changes in surface fluxes implied by the alteration to the model are important, and these changes have implications for the flux adjustments necessary when the LSG model is coupled to an atmosphere model. The results presented here indicate considerable scope for reducing such flux adjustments.

1. Introduction

Climate is continually variable on all timescales. A knowledge of this natural variability is important for a number of climatological problems, including (i) the detection of an anthropogenic climate change signal against this background variability (Santer et al. 1996), (ii) the estimation of climate sensitivity by fitting a transient climate model to the observed temperature record (Wigley and Raper 1991), (iii) the validation of climate models in addition to the usual validation of the mean state, and (iv) the ability to prepare for and/or predict such natural variability.

While the instrumental record can be used to provide this knowledge on interannual timescales (Jones 1989) and on interdecadal timescales for limited regions (Trenberth 1990; Kushnir 1994; Schlesinger and Ramankutty 1994), they can say little about intercentennial variability. A range of climate proxy records exist (Stocker and Mysak 1992) that add useful information, but their limited spatial coverage, the few climate variables obtainable, and the difficulty involved in removing the influence of nonclimatic effects or separating the effects of multiple climate variables all tend to reduce their utility. Given these limitations, it is necessary to augment the instrumental and proxy records with model results.

On interdecadal and intercentennial timescales, it is likely that the ocean plays an important role since its thermal inertia gives it a response time within that range. This role might simply be passive (e.g., Wigley and Raper 1990) or it might actively generate climate variability (e.g., Mikolajewicz and Maier-Reimer 1990, hereafter MM90).

Ideally, the model should also include a realistic representation of the atmosphere (and of the cryosphere, biosphere, nutrient and chemical cycles, and of solar and orbital variations), but that demands the availability of tremendous computational resources. Some preliminary coupled ocean–atmosphere general circulation model (GCM) investigations have now been made on

Corresponding author address: Dr. Timothy J. Osborn, Climatic Research Unit, University of East Anglia, Norwich NR4 7TJ, United Kingdom.
E-mail: t.osborn@uea.ac.uk

these long timescales (e.g., Delworth et al. 1993; Stouffer et al. 1994; Lunkeit et al. 1996; Schneider and Kinter 1994; von Storch 1994; Mitchell et al. 1995). These integrations are of great importance, but there remain some problems with them (e.g., model drift, the possible effect of flux correction) and they may not yet simulate as much variability as is observed in the real world (Barnett et al. 1996b). For the longer timescales, and for more exhaustive investigations (including the parameter and resolution sensitivity of any variability obtained), either uncoupled OGCMs (e.g., MM90) or OGCMs coupled to simple atmosphere models (e.g., Pierce et al. 1996) must be used.

The work reported in this paper is a further extension of the MM90 study. They showed that the Hamburg Large-Scale Geostrophic (LSG) OGCM (Maier-Reimer et al. 1993) exhibited pronounced variability with a 320-yr timescale when integrated under mixed boundary conditions and forced by stochastic fluxes of freshwater. They identified the Atlantic and Southern Oceans as being the principal regions involved in the oscillation and suggested that the advective timescale of Atlantic meridional overturning controlled the period of the oscillation. Pierce et al. (1995, hereafter PBM95) extended this work by identifying a mechanism for the generation of the variability that is entirely a Southern Ocean process.

To ascertain whether this variability might have a counterpart in the real oceans, a number of uncertainties must be addressed. First, does the variability occur in models that also include a representation of the atmosphere? This is the subject of a number of other studies (Mikolajewicz and Maier-Reimer 1994; Osborn 1995; Pierce et al. 1996; Osborn et al. 1997, unpublished manuscript, hereafter OBW) and it is not considered here (except during the discussion of the feedback processes and atmospheric feedback in section 2). Second, what is the driving mechanism—MM90's Atlantic overturning or PBM95's Southern Ocean flip–flop? That is the subject of section 4 of this paper, where another mechanism of possible importance is also identified. There, analysis of Atlantic signals is presented, and upper-ocean salinity budgets of the Southern Ocean are constructed. Third, how sensitive is the existence of the variability to the model's formulation in terms of its resolution, numerical schemes, and physical parameterizations? Some of the latter questions are answered in section 5 by making changes to the model's formulation (equations of motion, convection, and ice–ocean coupling) and repeating a standard experiment.

2. Mixed boundary conditions and the convective feedback

The experiments reported in MM90 and PBM95 were performed under mixed boundary conditions. That is, the freshwater flux was held fixed (except for a seasonal cycle and the addition of noise) while the heat flux was computed from a relaxation boundary condition (Haney 1971) on sea surface temperature (SST) toward a prescribed air temperature. The rationale for using such conditions is that the net surface freshwater flux should have no direct dependence on the surface salinity, whereas any small SST anomalies will induce net surface heat flux anomalies of the appropriate sign to remove the SST anomalies. These heat flux anomalies do not, by design, alter the prescribed air temperature—a condition that may be reasonable for small heat anomalies that can be rapidly removed by atmospheric advection, diffusion, and longwave radiational cooling. As Haney (1971) notes, though, the relaxation boundary condition on SST is only applicable for small departures from the climatological mean. This restriction is broken by the LSG experiments that exhibit pronounced 320-yr oscillations (including MM90, PBM95, and the present study).

To understand why the breaking of this restriction may have a large effect on the simulated variability, it is necessary to understand the processes that drive the variability. A main driving process is the rapid amplification of sea surface salinity anomalies (SSSA); this amplification is particularly strong when mixed boundary conditions are used. Stommel (1961) first described such feedbacks in a North Atlantic situation where horizontal advection is important; Power (1995) and Drijfhout et al. (1996) described the ''convective feedback'' as the equivalent process in the Southern Ocean where the lack of zonal boundaries allows vertical processes to dominate.

In regions of convective activity that also have a net input of freshwater at the surface (northern North Atlantic and parts of the Southern Ocean), there is an increase in salinity and temperature with depth [in both the real ocean (Levitus 1982) and in model simulations (Maier-Reimer et al. 1993, their Fig. 7)]. Convective overturning of these water columns results in a flux of heat and salt from the subsurface ocean to the surface. The heat is lost to the cooler atmosphere, and the salt flux is offset by the freshening effect of the air–sea freshwater flux; a steady state is thereby obtained. If a small negative SSSA is introduced, it will lower the surface water density slightly, thereby reducing convective activity. As a result, the convective fluxes of heat and salt will be reduced, further freshening the surface—but cooling it too. If the SST boundary condition involves a strong relaxation to some fixed temperature, then the cooling will be offset by induced surface heat fluxes, leaving the enhanced surface freshening alone to further affect the density and convective activity. This is the convective feedback.

The slight cooling of the upper ocean provides a further positive feedback (PBM95) since the nonlinear equation of state strengthens the stabilizing effect of the vertical salinity gradient relative to the destabilizing temperature effect as the water cools. Similar arguments

can demonstrate that both positive feedbacks act on positive SSSA too.

These positive feedbacks amplify any salinity anomalies that appear in the convectively active regions, and it is these feedbacks that drive the variability found by MM90. (The mechanism by which the ocean recovers—and hence oscillates—following the amplification of anomalies of one particular sign has been described by PBM95.) The important point is that the strength of these feedbacks is dependent upon the strength of the relaxation boundary condition on SST (i.e., on its ability to restrain SST changes and allow salinity changes to dominate in controlling convective activity), and they only act in a positive sense if the relaxation is sufficiently strong. This strength is quantified by the coupling coefficient (γ), relating air–sea heat flux to air–sea temperature difference.

The coupling coefficient used here (and by MM90 and PBM95) appears to be realistic [40 W m^{-2} K^{-1}—equivalent to a relaxation timescale of 60 days—compared to the observationally based estimate of Oberhuber (1988) of 35–40 W m^{-2} K^{-1} in the annual and global mean]. The problem is with the use of a fixed air temperature. In reality, air temperature will respond to the anomalous air–sea heat flux; the resulting air temperature anomaly will usually be of the same sign as the SST anomaly and will thus be a weaker constraint on SST variations. Traditional mixed boundary conditions can, therefore, be improved upon in one of two ways: either couple the ocean to an atmosphere model that allows air temperature to vary or reduce the coupling coefficient to compensate for a fixed air temperature.

Focusing on the North Atlantic, Zhang et al. (1993), Power and Kleeman (1994), and Mikolajewicz and Maier-Reimer (1994) have confirmed a weakening of the feedback processes when the coupling coefficient is reduced. Coupling to an implicit energy balance model (EBM), Rahmstorf and Willebrand (1995) found a similar reduction in feedback strength. It is not certain, however, if the weaker constraint on SST is sufficient to prevent the feedback from operating in a positive sense. Rahmstorf (1995) still found some variability in his coupled model, while the reduction in γ suggested by supplying characteristic-scale SST anomalies to atmosphere models [Seager et al. (1995) obtained 15 W m^{-2} K^{-1}; Mikolajewicz and Maier-Reimer (1994) obtained 16 W m^{-2} K^{-1}; Osborn (1995) obtained 20 W m^{-2} K^{-1} in the high latitudes] does not appear sufficient to achieve complete thermohaline stability.

Focusing on the Southern Ocean variability in the LSG OGCM, Mikolajewicz and Maier-Reimer (1994) showed greatly reduced variability when γ was reduced to 16 W m^{-2} K^{-1} and different noise forcing was used. They do not show, however, whether this reduction in variability was solely due to the change in γ.

Pierce et al. (1996) found inconclusive results when coupling an atmosphere EBM to the LSG OGCM. Some cases oscillated strongly while others were unvarying, depending upon model tuning, flux correction, and the details of the freshwater flux forcing/noise. The case with the least variability (and presumably the weakest convective feedback) found by Pierce et al. (1996) is probably unrealistic. They reduced the coupling coefficient between SST and the EBM's air temperature from 40 W m^{-2} K^{-1} to 20 W m^{-2} K^{-1}, which stabilized the circulation in all cases. They misinterpret, however, the work and recommendations of Seager et al. (1995). They recommend that, if a reduction in the coupling coefficient is used rather than an atmosphere model (that can develop its own scale-dependent coupling), then γ should be about 15 W m^{-2} K^{-1}. They do not suggest that the coupling coefficient between an OGCM and an atmospheric model that allows air temperature to vary should be reduced to that level, as Pierce et al. (1996) did.

The LSG OGCM has also been coupled to a statistical atmosphere model, based on the spatial and local relationships between SST and air–sea fluxes displayed during an AGCM simulation (Osborn 1995; OBW). Allowing air temperature to vary in this hybrid coupled model does indeed weaken the convective feedback on salinity—but not completely. The feedback still operates, and thermohaline circulation variability still occurs, albeit considerably weaker in magnitude (Osborn 1995; OBW).

Coupling the LSG model to an AGCM (von Storch 1994), little variability of the type found in the uncoupled LSG OGCM was apparent, although it underwent considerable climate drift in the Southern Ocean that could have led it to a state where this type of variability was unable to occur. The evidence from O/AGCMs is not yet conclusive: some find variations for which salinity feedbacks are likely to be of importance (e.g., Manabe and Stouffer 1988; Lunkeit et al. 1996), while others do not (e.g., Delworth et al. 1993; Mitchell et al. 1995).

To summarize, it remains uncertain whether the LSG OGCM will exhibit similar thermohaline variability when air temperature is realistically modeled compared to when mixed boundary conditions are used. If it does, then the mixed boundary condition experiments will still be applicable. If it does not, then the experiments presented here will be of less direct relevance; their relevance will come from the fact that the LSG OGCM is particularly sensitive (to changes in model formulation, boundary forcing, etc.) when integrated under mixed boundary conditions, and this provides a useful test bed for assessing the effect of changes to the model.

3. Description of the LSG OGCM

The development, structure, and performance of the Hamburg Large-Scale Geostrophic OGCM are described in detail by Maier-Reimer et al. (1993 and references therein). The configuration used here is virtually identical to that used by MM90 and PBM95.

The LSG model has been specifically designed for

climate studies, where a global model capable of long integrations is required. The main assumptions are that the spatial scales to be studied are large compared to the internal Rossby radius of deformation (~50 km) and that the temporal scales in climate studies are large compared to the periods of gravity waves and barotropic Rossby waves. The primitive equations are used with the hydrostatic and Boussinesq approximations applied. On the basis of the two assumptions (above), the nonlinear advection of momentum is removed from the primitive equations. This is the main difference between the LSG OGCM and other OGCMs, and gives the model its name—since the resulting equations describe a quasigeostrophic flow. The second assumption (above) allows the fast modes to be filtered, which is done by integrating the model equations with a long-time-step implicit scheme. A 30-day time step is used here.

Sea surface elevation is prognostic, a full equation of state is used, and a simple sea ice model is included. The latter is thermodynamic, and ice is advected by the surface ocean currents. A convection scheme removes static instabilities by interchanging the water mass characteristics of the levels involved, although complete stability is not ensured. Geometry and bathymetry are as realistic as the 3.5° lat by 3.5° long horizontal resolution allows. Eleven unequally spaced levels are used in the vertical (centered at depths 25, 75, 150, 250, 450, 700, 1000, 2000, 3000, 4000, 5000 m).

Seasonally varying wind forcing from Hellerman and Rosenstein (1983) is used to force the OGCM. As discussed in section 2, mixed boundary conditions are used: model SST is relaxed to a COADS-based air temperature (Woodruff et al. 1987) with a relaxation timescale of 60 days; and a fixed air–sea freshwater flux is applied. The latter represents the net total of precipitation, evaporation, and runoff; it is not observationally based, being diagnosed from an earlier spinup integration during which sea surface salinity was relaxed to observed salinity (Levitus 1982).

4. Propagating anomalies

a. The Atlantic signals

In their initial analysis of the variability of the LSG OGCM, MM90 concentrated on the propagation of positive and negative salinity anomalies around the meridional overturning circulation of the Atlantic Ocean. Salinity anomalies travel around the meridional circulation of the Atlantic Ocean: northward in the upper ocean, southward in the deep ocean. Amplification by the convective feedback occurs when the anomalies are at the surface of the convectively active high latitudes.

MM90 suggest that this cycle controls the period of the oscillations. But PBM95, who have offered the most convincing explanation yet of the mechanism that generates these oscillations, hardly consider the Atlantic signals at all; their mechanism is a Southern Ocean one. Simply put, following the amplification of a negative surface salinity anomaly in the Southern Ocean by the convective feedback, the effect of subsurface warming on the density field (both the direct effect and indirectly through the nonlinear equation of state) eventually destabilizes the water column and restarts convection from below (see PBM95 for further details).

It remains uncertain which one of these mechanisms is important (or both). This uncertainty is resolved by performing a simulation in which no salinity signals are allowed to propagate around the Atlantic overturning circulation. This is achieved by relaxing Northern Hemisphere sea surface salinity toward the observed field with a relaxation time constant of 40 days. This strongly damps Northern Hemisphere sea surface salinity anomalies. Mixed boundary conditions were maintained in the Southern Hemisphere. This simulation is compared with the ''standard'' simulation in which mixed boundary conditions are applied everywhere; that is, there is no relaxation upon salinity at all.

In order to excite any internal variability, identical noise forcing is applied to the freshwater flux in both simulations (although it is damped by the relaxation applied to the Northern Hemisphere in one simulation). This noise is a combination of white noise (spatially and temporally incoherent with a uniform standard deviation of 30 mm mo^{-1}) and red noise (spatially and temporally coherent) derived from a simulation with the ECHAM3 AGCM (see Osborn 1995, for details).

The variability in these model simulations is characterized by the strength of the Antarctic Circumpolar Current (ACC) through the Drake Passage (Fig. 1), because changes in Southern Ocean convection affect the density structure and the sea surface elevation gradient across the ACC (PBM95 compare the signal of variability in the ACC and in the overturning strength). The most important result is that oscillations of the LSG model's thermohaline circulation still occur in the simulation with the Northern Hemisphere salinity relaxation condition, despite the prevention of any signal propagation around the Atlantic Ocean (Fig. 1b). The period of the oscillations is approximately 300 yr, compared to a 320-yr periodicity for the standard mixed boundary conditions simulation (Fig. 1a). The character of the variability appears to be little changed. It is likely, therefore, that the mechanism of PBM95 is the key process for the existence of these thermohaline oscillations in the LSG OGCM.

But what of the salinity anomalies that propagate around the Atlantic meridional overturning circulation? For the standard mixed boundary conditions simulation, these are shown for one 400-yr period at the surface (Fig. 2a) and in the deep ocean (Fig. 2b). These figures show the time evolution of the salinity anomaly field along a section from Antarctica to the North Pole that approximately follows the western boundary currents of the Atlantic Ocean.

During the high ACC period of the standard simulation (4820–5000, see Fig. 1a), strong convection increases the flux of salt (and heat) up to the surface of the Southern

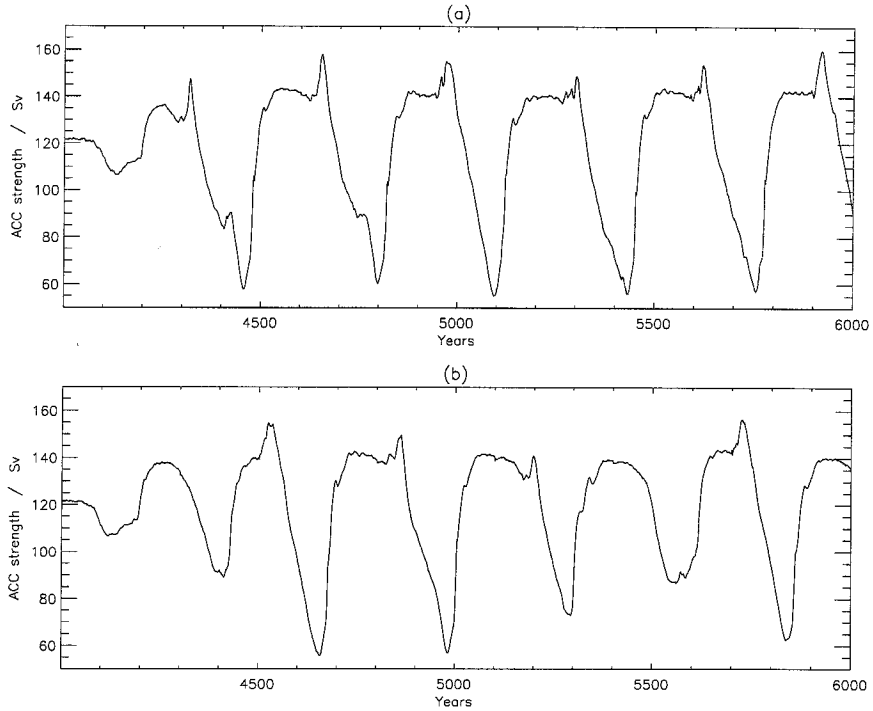

FIG. 1. Antarctic Circumpolar Current strength (Sv) from 2000-yr mixed boundary condition simulations (a) forced by freshwater flux red and white noise; (b) as in (a) but with a relaxation boundary condition used on surface salinity in the entire Northern Hemisphere.

Ocean, thereby creating positive sea surface salinity (SSS) anomalies in the Southern Ocean (Fig. 2a). The salty anomaly is advected northward into the Atlantic Ocean, becoming weaker, and reaching 35°N within 80 yr of its creation (Fig. 2a). After a delay of 120 yr, the SSS anomaly reaches the northern North Atlantic and is amplified (50°N, year 5040) by the convective feedback (although it remains weaker than it was in the Southern Ocean). Negative SSS anomalies behave similarly, being created in the Southern Ocean when the ACC is weak (5000–5120) and there is little convection occurring.

When the positive sea surface salinity anomaly reaches the convective region of the North Atlantic (year 5040), it is advected/convected down to the deep ocean to create a positive salinity anomaly there (Fig. 2b). This anomaly reaches a maximum soon after. It propagates quickly southward through the deep Atlantic Ocean, as shown by MM90. They argued that it may be involved in triggering the next oscillation when it eventually reaches the deep Southern Ocean. At 30°S, however, a positive anomaly of equal magnitude appears to develop (year 5070) *before* the anomaly propagating from the northern North Atlantic has even reached 10°N. It is shown below that the anomalies at 30°S develop independently of the anomalies traveling from the North Atlantic Ocean.

Negative deep ocean salinity anomalies behave similarly, although the negative salinity anomaly that occurs in the deep ocean at 30°S reaches a magnitude (-0.06 psu) three times stronger than the northern North Atlantic anomaly (Fig. 2b).

Results from the simulation with the Northern Hemisphere salinity relaxation condition are shown in Fig. 3. Both positive and negative SSS anomalies are generated in the Southern Ocean (Fig. 3a) and propagate northward as before. When they reach and pass the equator, they are rapidly removed by the relaxation boundary condition. No surface salinity anomalies of significant size reach, or are generated, in the northern North Atlantic. Hence, no salinity anomalies are input into the deep ocean via NADW formation, and deep Atlantic Ocean salinity anomalies are very weak poleward of 40°N. Despite this, very strong salinity anomalies are still generated in the deep ocean at 30°S (Fig. 3b). These anomalies, therefore, are independent of the anomalies that propagate southward from sites of NADW formation. Once created, the deep 30°S anomalies propagate southward (and northward too).

The simulations of Mikolajewicz and Maier-Reimer (1990) also contain the same 30°S feature. Their Fig. 10 shows that salinity anomalies at 30°S and 3000 m depth do develop up to 80 yr *ahead* of the anomalies propagating from the North Atlantic Ocean (this is particularly clear for the negative salinity anomalies).

Salinity anomalies are created in the deep South Atlantic, therefore, regardless of the propagation of anomalies around the Atlantic overturning circulation. They are cre-

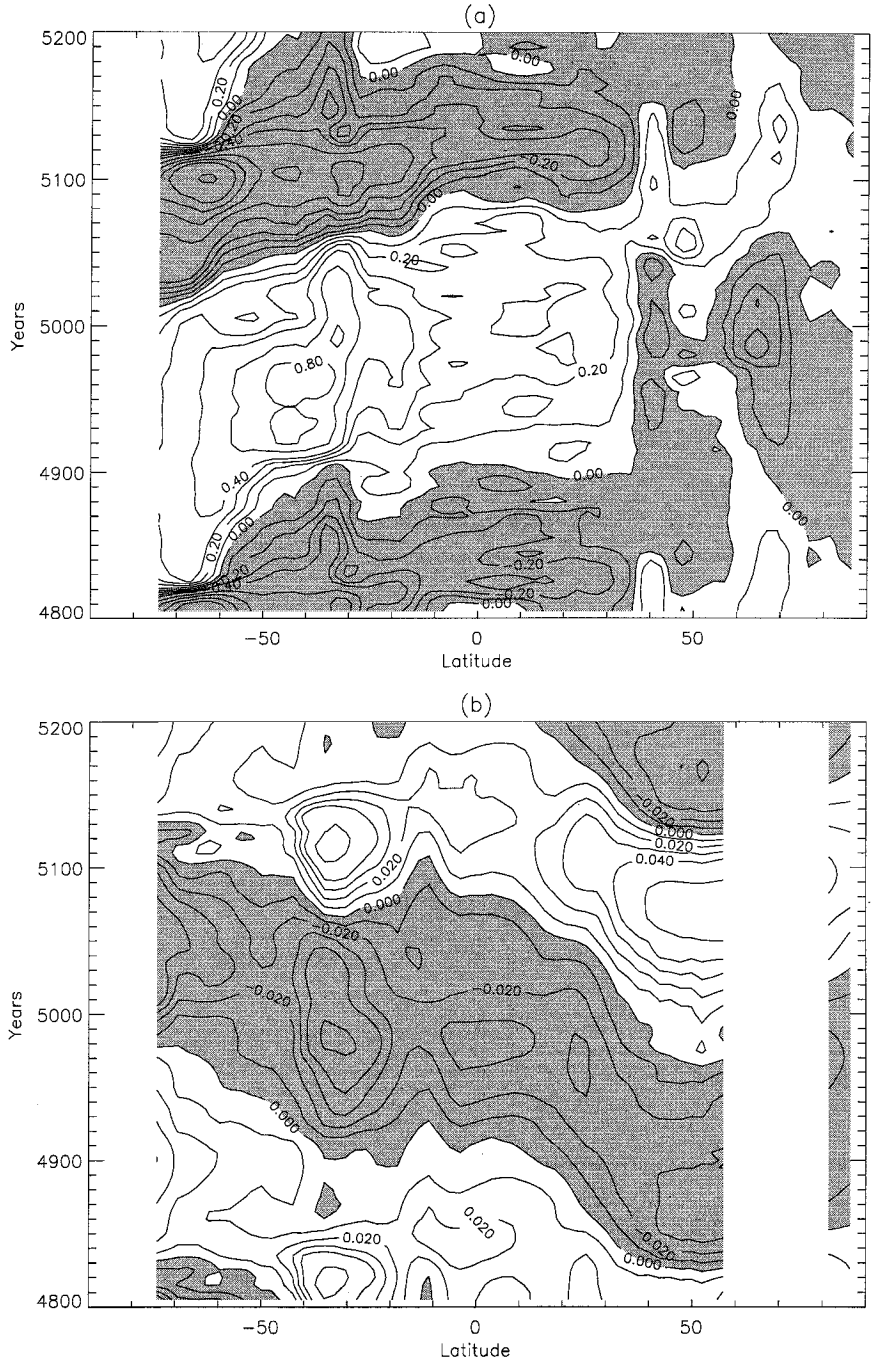

FIG. 2. Evolution of (a) surface and (b) deep ocean salinity anomalies (psu) on a meridional section near to the western boundary of the Atlantic Ocean, from a 400-yr period of the simulation shown in Fig. 1a. Negative anomalies are shaded.

ated in situ by a reversal of the meridional flow at this depth in response to anomalous density gradients in the upper ocean related to the next phase of the variability at the surface (see Osborn 1995, for further details). Whether these deep anomalies play any role in triggering the next oscillation has not been ascertained, but they are not necessary according to the PBM95 mechanism.

b. The Antarctic signals

In the previous section, it was confirmed that the 320-yr variability in the LSG OGCM is entirely a Southern Ocean phenomenom, as argued by PBM95. Their mechanism involves a flip–flop oscillator (e.g., Welander 1982) in the Southern Ocean deep-water for-

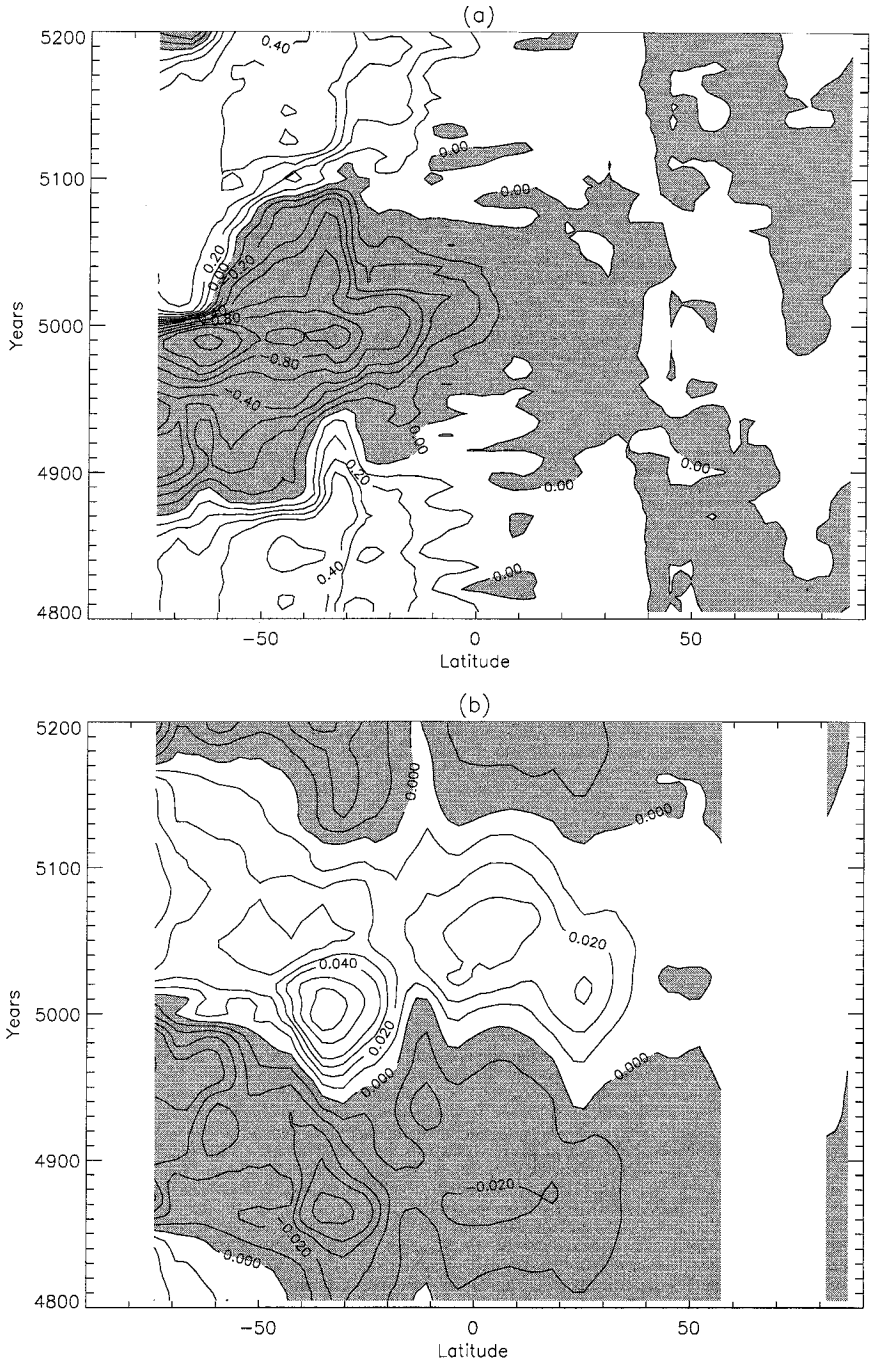

FIG. 3. As in Fig. 2 but from a 400-yr period of the simulation shown in Fig. 1b.

mation regions. When any small, negative SSS anomalies are amplified by the convective feedback, a freshwater cap rapidly reduces convective overturning. Heat is no longer vented from the subsurface ocean which consequently warms. The effect of this warming on the nonlinear equation of state eventually overcomes the stabilizing effect of the freshwater cap and convection restarts, triggered from below.

This mechanism is now investigated further to discover whether these processes operate independently at all locations around Antarctica or whether any linkages (i.e., signal propagation) exist longitudinally. To facilitate this exercise, the Southern Ocean poleward of 60°S is split into five sectors (Fig. 4, following PBM95) in which salinity budgets will be analyzed. Salinity is the controlling variable for the oscillations, and the budgets will help to ascertain whether it is controlled purely by local processes or whether salinity signals communicate between sectors.

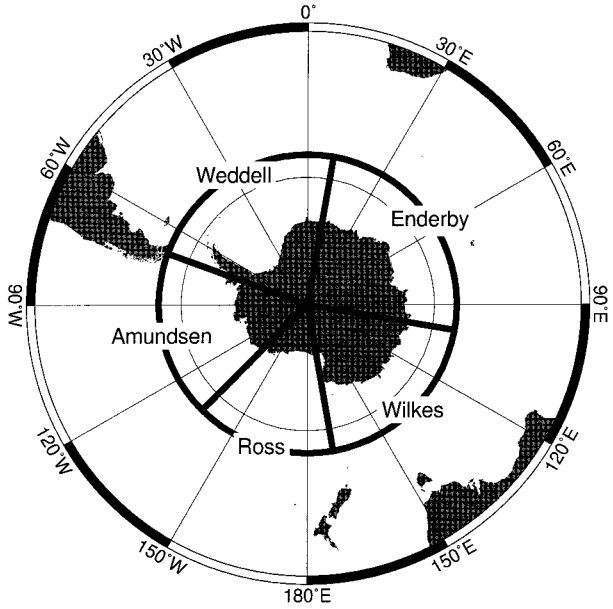

FIG. 4. Definition of Antarctic sectors.

A surface salinity budget for the Weddell sector was first constructed (Fig. 5) for the same 400-yr segment of the noise-forced mixed boundary conditions simulation discussed in the previous section (Figs. 1a and 2). The budget is divided into four salinity tendency terms: net surface freshwater flux, the effect of sea ice, the flux due to convective overturn, and a combined advective and diffusive flux (all directions, including vertically).

This budget is of the *combined* salinity of the uppermost layer of water *and of the sea ice* (assumed to have zero salinity in this version of the LSG OGCM, but its nonzero thickness affects the mean salinity). Using the combined ice and water salinity for the budget automatically includes the contribution of sea ice import/export in the advection plus diffusion component. Moreover, the salinity tendency due to the freshwater flux (FWF) will be properly accounted for, whether it goes into the water or lands on the ice. It goes entirely into the water or entirely onto the sea ice depending upon whether the sea ice is less than or more than 0.1 m thick; in either case, it appears in the FWF term and never in the sea ice term.

This budget highlights a number of interesting points. The cycle of salinity during one thermohaline oscillation is quite clear (Fig. 5a) and shows few higher frequency variations of any significance. The start and end years of the periods of salinity decrease (years 4950 to 5095) and increase (years 5095 to 5135) are more precisely determined from the annual change in the salinity (Fig. 5b).

The salinity tendency due to air–sea fluxes (Fig. 5c) is the only negative (i.e., freshening) term; the others are all positive. The white noise forcing added to the freshwater flux in this simulation is the cause of the high-frequency changes in this term (Fig. 5c). There are also some low-frequency variations in this term, not due to the red noise forcing since that is confined mainly to the Tropics, but because of changes in sector salinity and mass content (i.e., layer thickness plus ice thickness variations; the LSG OGCM has a free surface). The salinity tendency due to the freshwater flux is dependent upon these two variables as well as on the magnitude of the flux itself. The influence of these other two variables has only been removed on an annual and sector mean basis; intrasector and intraannual covariation of salinity and mass content results in the small low-frequency variations that remain in the salinity tendency due to FWF (Fig. 5c).

The salinity tendency due to the sum of advective and diffusive fluxes (Fig. 5e) shows variability on many timescales, but the changes are weaker than in the other positive terms. The amplitude of variations due to changes in convective activity (Fig. 5f), for example, is twice as large.

The salinity tendency due to the effect of sea ice changes (Fig. 5d) is (surprisingly) positive, and is also very strong. This term was expected to be negative because the budget is of the combined salinity of the surface water layer and of the sea ice. If sea ice melts, there should be no change in the salinity, since this just shifts the partition between ice and water, but not the total mass or salt. During freezing of water to produce sea ice, brine is rejected into the water. The brine rejected into the *uppermost* layer does not affect the combined ice and water salinity. However, Maier-Reimer and Mikolajewicz (1992) indicate that a portion of the brine should sink to the *second* model layer down and appear as a salinity loss in the budget. This latter process is clearly not occurring, and salt is, in fact, being moved upward from the second model layer into the surface layer as a result of the sea ice model. (This is probably unrealistic and is addressed in detail in section 5c of this paper.)

The decrease in surface salinity from year 4950 to 5095 was due to a decrease in the convective flux of salt from the subsurface ocean to the surface (Fig. 5f)—that is, the convective feedback in operation. According to the flip–flop oscillator of PBM95, the subsequent increase in salinity should be driven by a renewal in convective activity. In this sector, however, convective activity completely stops in year 5073 and does not restart again until 5108—almost 15 yr after the salinity begins to rise. Instead, it is an increase in the salinity tendency due to the sea ice model that causes the rise in surface salinity. As discussed above, this term involves a transfer of salt from the second model layer up to the surface and increases in year 5095 due to an increase in the salinity of the second model layer down (at a depth of 75 m). A similar budget of this subsurface layer (not shown) confirms this rise and shows that it is not due to a restart in convective activity either. The

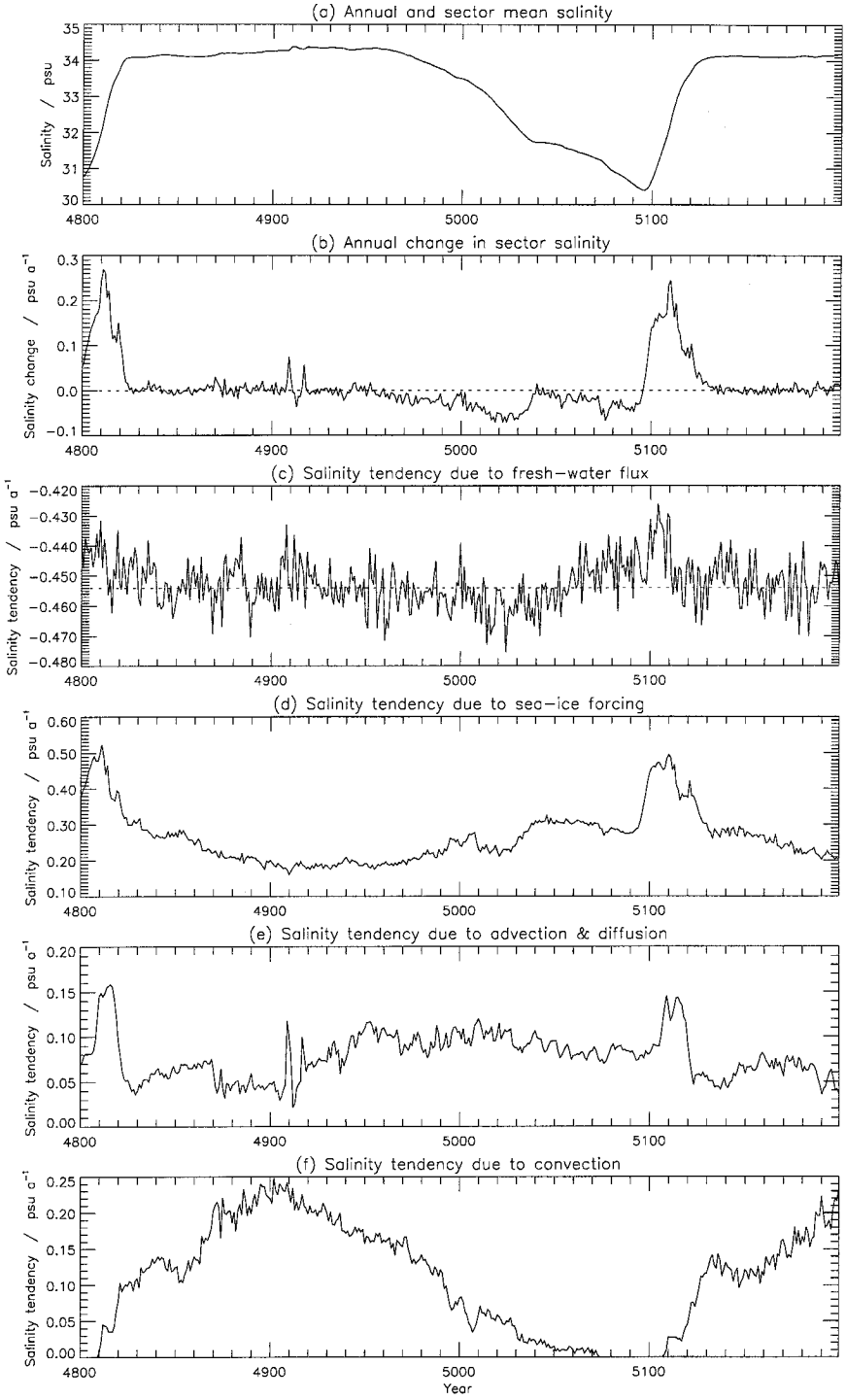

FIG. 5. Annual surface salinity budget (psu yr^{-1}) for Weddell sector for a 400-yr section of the simulation shown in Fig. 1a. (a) Salinity (psu), (b) annual change in salinity, (c) corrected salinity tendency due to FWF, (d) salinity tendency due to sea ice forcing, (e) salinity tendency due to vertical and horizontal advection and diffusion, and (f) salinity tendency due to convection.

change that precedes the 75-m salinity rise is in the advection/diffusion term, which increases strongly in year 5095. Almost simultaneously, the sea ice term takes this extra salinity away and puts it in the uppermost layer, as seen in the surface budget (Fig. 5d).

Analysis of salinity changes (not shown) in the areas to the west, east, and north of the Weddell sector, as well as in the next layer down, indicates that it is the Enderby sector to the east (Fig. 4) that is the source of the increased advective/diffusive flux of salt into the Weddell sector at a depth of 75 m. Budgets of the salinity of the upper two model layers of the Enderby sector show a similar cycle in salinity, with the formation of a surface freshwater cap coinciding with a reduction in convective activity. For this sector, however, the subsequent recovery in salinity *is* driven by a renewal in convective overturning.

The flip–flop mechanism of PBM95 does appear to hold in the Enderby sector where the surface freshwater cap is eventually removed by renewed convection, itself caused by subsurface warming. Some of the more saline water that replaces the freshwater cap propagates westward to the Weddell sector and begins to raise the upper-ocean salinity there a decade later. Nearly 15 yr later, the increase in upper-ocean salinity is sufficient to restart Weddell sector convection, from above rather than by subsurface warming from below (as argued by PBM95).

This is only a slight refinement to the sequence of events proposed by PBM95 since they had already stated that convection restarts in the Enderby sector first. Further, while it is the transport of salt from the Enderby sector that triggers renewal of Weddell sector convection, the subsurface warming that had also occurred was still of great importance; without it, the rise in salinity would not have been sufficient to restart convection. This new work does raise two important points, though. First, it highlights the longitudinal interconnections between the variability in the Antarctic sectors. Second, it raises the question of how salinity anomalies move westward from one sector to the next.

The westward propagation of surface salinity anomalies is depicted by four snapshots of the model's Southern Ocean, each separated by 5 yr (Fig. 6, left-hand column). These are salinity anomalies referenced to year 5070, a time when there was little convective activity (Fig. 1a) due to the existence of a freshwater cap over much of the Southern Ocean (Fig. 2). In year 5095 (Fig. 6, top left panel), subsurface warming has restarted convection in the Enderby sector (Fig. 4, south of the Indian Ocean) and replaced the freshwater cap with more saline subsurface water (unshaded anomaly). The subsequent propagation of this positive salinity anomaly to the west is evident (Fig. 6, subsequent panels of the left column), reaching the Weddell Sea after 15 yr (Fig. 6, bottom left panel).

The main difficulty in understanding how the anomalies move westward is that the ACC flows eastward with considerable strength, and the westward flowing Antarctic Coastal Current is not correctly simulated by the LSG model. Simple advection is, therefore, ruled out.

Drijfhout et al. (1996) have recently found a non-advective westward propagation mechanism for salinity anomalies around the Antarctic coast in the Hamburg Ocean Primitive Equation (HOPE) OGCM. This mechanism requires salinity to increase with depth in the upper few hundred meters, a profile representative of much of the Southern Ocean in both the real world and the LSG OGCM.

The Drijfhout mechanism can be summarized as follows. A positive salinity anomaly in the upper ocean of the Southern Hemisphere causes an anticyclonic geostrophic flow anomaly (Fig. 7a) that is not closed if it is adjacent to the Antarctic coast (Fig. 7b). Continuity induces coastal upwelling to the west of the anomaly and downwelling to the east. Due to the ambient vertical salinity gradient, the upward velocity anomaly brings up saltier water from below, increasing the salinity to the west of the initial anomaly. This effectively extends the salinity anomaly to the west (Fig. 7c). In the HOPE model, the downwelling to the east apparently results in a freshening there, and the salinity anomaly actually moves westward (Fig. 7d) rather than just extending westward (Fig. 7c). Currently, in the LSG model the salinity anomaly is not simply an isolated coastal anomaly, so that the situation would be more like that sketched in Fig. 7e.

The Drijfhout mechanism also operates in the LSG model since an upward velocity anomaly leads the salinity anomaly and a downward velocity anomaly follows it during its propagation. Four snapshots of the model's vertical velocity anomaly field (unshaded implies upward) in the Southern Ocean are shown in Fig. 6 (right-hand column). These are at a depth of 112.5 m, also referenced to year 5070, and are at the same times as the salinity anomalies shown in the left-hand column (year 5095 to 5110) in 5-yr steps.

Before 5095, the main positive salinity anomaly south of the Indian Ocean was moving southward. At 5095 (Fig. 6, top left panel), it reached the Antarctic coast and induced an upward velocity anomaly to its west and a downward velocity anomaly to its east (Fig. 6, top right panel—ignore the Drake Passage anomalies for now, which are unchanging). The vertical velocity anomalies are quite difficult to discern because they are very close to the Antarctic coast—in accordance with the mechanism shown in Fig. 7. The upward velocity anomaly at the western edge of the positive salinity anomaly induced a westward extension of the salinity anomaly (left, second panel) by the mechanism described above. The unshaded upward velocity anomaly (right, second panel) then moves farther west—at the new leading edge of the salinity anomaly. The mechanism then continues, but now farther west, with an upward velocity anomaly maintained at the leading edge of the salinity anomaly.

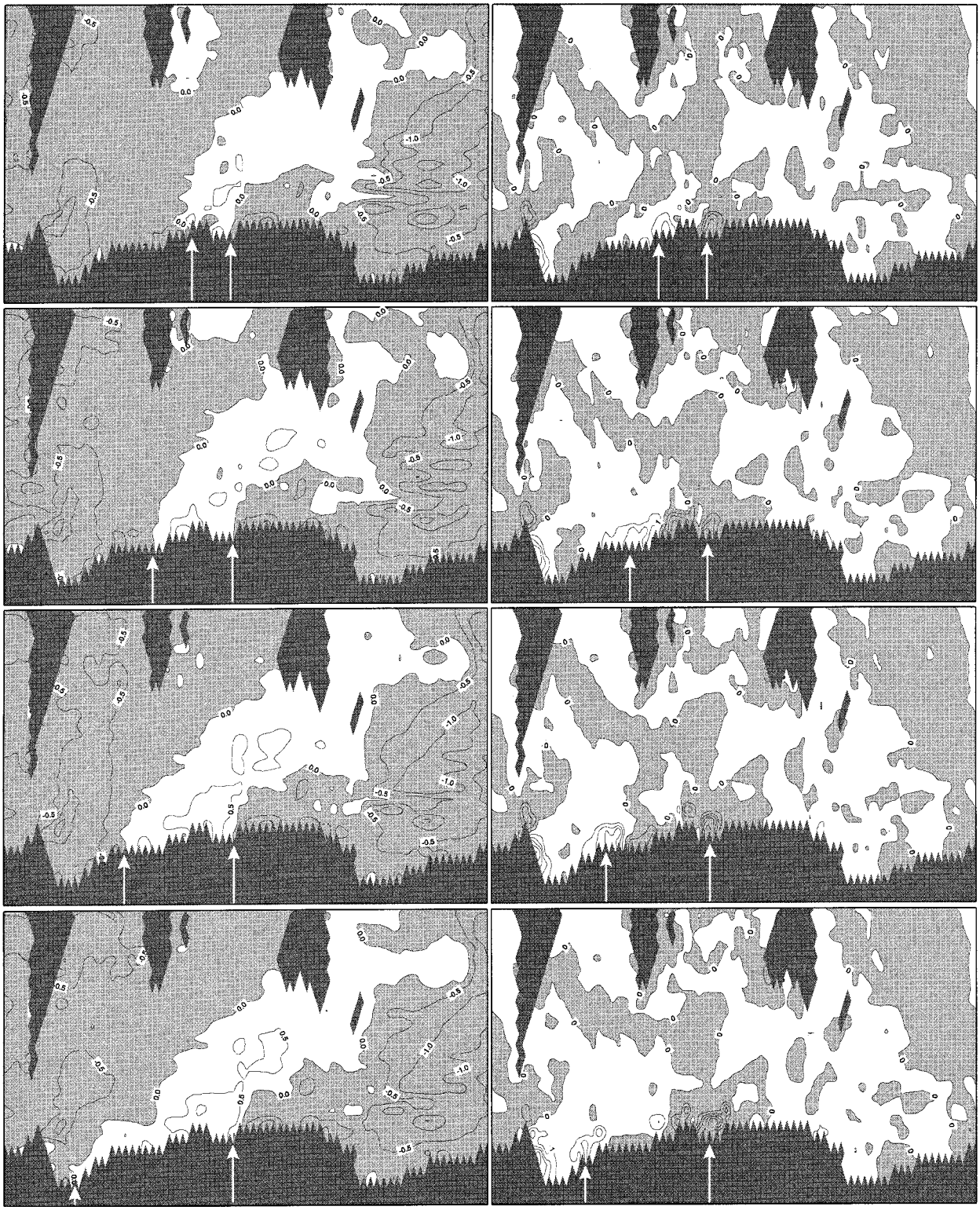

FIG. 6. Anomaly patterns from the simulation shown in Fig. 1a referenced to year 5070. Negative anomalies are shaded. (Left column) 25-m salinity anomaly, isoline interval 0.5 psu. (Right column) 112.5-m vertical velocity anomaly, positive upward, isoline interval 10^{-6} m s^{-1} (= 31 m yr^{-1}). (Top panels) year 5095. (Second panels) year 5100. (Third panels) year 5105. (Bottom panels) year 5110. Arrows indicate key features (see text).

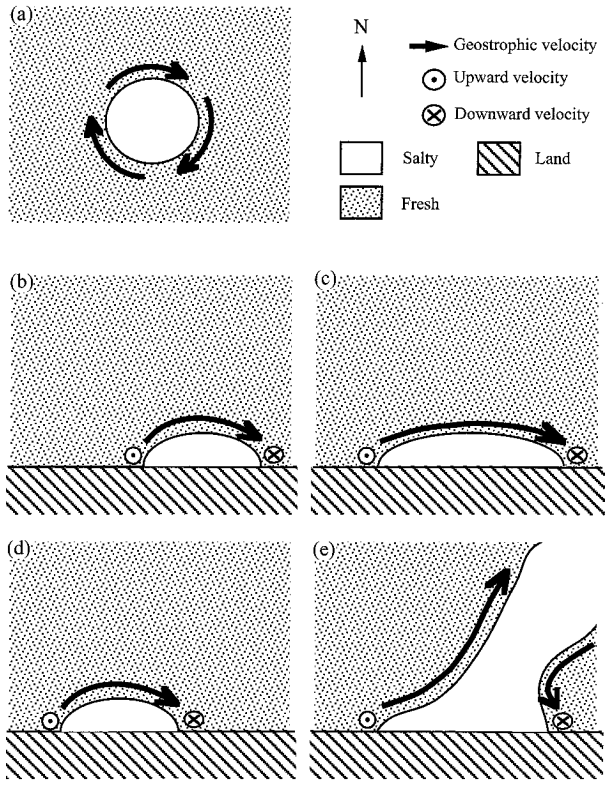

FIG. 7. Schematic diagram of propagation mechanism. (a) Response to an open-ocean salinity anomaly. (b) Response to an upper-ocean salinity anomaly adjacent to Antarctica. (c) Extension of salinity anomaly by upwelling of saltier water. (d) Movement of salinity anomaly by freshening to the west, caused by the induced downwelling. (e) Situation in the LSG model, where the anomaly extends far from the coast.

The signal propagates even farther west, through the Drake Passage where the strong eastward flowing ACC is immediately adjacent to the Antarctic coast in the LSG model. In fact, the anomaly propagates as far as the Ross Sea, although at a slower velocity (it takes 15 yr to move 90° of longitude from the Enderby to the Weddell sector, yet an additional 150 yr to progress an additional 180° of longitude to the Ross Sea).

Once formed, the salinity anomaly is maintained because it raises the surface density sufficiently to trigger convection. Through the convective feedback, the SSSA is amplified. Triggering of convection only occurs if subsurface warming has lowered the static stability to a critical level. The SSSA reaches the Amundsen sector before the static stability has reached this critical level (in the mean state, this sector has a much stronger freshwater cap to overcome). As a result, the surface density anomaly was not amplified and was not sufficiently strong to induce leading-edge upwelling and the propagation halted. After 100 yr of additional subsurface warming, convection is triggered and the surface salinity anomaly is enhanced. When this occurs, an upward velocity anomaly is induced at its leading edge and westward propagation begins once more.

The eastern edge of the salinity anomaly remains stationary because the appearance of the anomaly and the resumption of convection destroy the freshwater cap, and the vertical salinity gradient becomes quite small. Vertical advective salinity fluxes are thus very weak and do not alter the salinity anomaly there.

In total, it takes 320 yr for a positive anomaly to extend westward from the Enderby sector around the whole of Antarctica (so that it fills the entire Southern Ocean, at which time the ACC has a maximum strength) and then to be completely removed by a negative salinity anomaly that also forms in the Enderby sector and propagates westward to once more cap the Southern Ocean (at which time the ACC is at a minimum). The correspondence between this apparent propagation timescale and the periodicity of the oscillations raises the possibility that the timescale of the oscillations is controlled by the propagation velocity. The importance of the subsurface warming and the convective feedback to the propagation mechanism does, however, mean that the reverse could be true. What is certain is that this propagation mechanism provides a link between the timing of the thermohaline oscillations at each longitude of the Southern Ocean.

The mechanism in the LSG OGCM is very similar to that identified in the HOPE model (Drijfhout et al. 1996). The two main differences are in the behavior of the eastern edge of the anomaly and in the propagation velocity. As sketched in Fig. 7d, the entire anomaly moves westward in the HOPE model, whereas the eastern edge is stationary in the LSG model (Figs. 7c and 6). The slow propagation of the LSG anomalies was discussed above and can be compared to the faster speed of just 20 yr for all 360° of longitude in the HOPE OGCM.

Comparison with the observed ocean is hindered by the paucity of time series of salinity and vertical velocity. The propagation of the positive (negative) salinity anomaly in the model is accompanied by induced negative (positive) sea ice thickness and sea surface elevation anomalies. These are more easily observed, but there is little in the literature that identifies a westward propagation of such anomalies. Lemke et al. (1980) found evidence for westward propagation of observed sea ice extent anomalies at some longitudes (although eastward elsewhere), but suggested that the westward propagation was simply an advective process.

This will, of course, be the main problem with finding observational evidence for any westward propagating signals: the real ocean does have a westward flowing Antarctic Coastal Current, so any observed propagation could be simple horizontal advection. Only if the observed propagation were inconsistent with simple advection (i.e., if its velocity were different from the observed current velocity), or if vertical velocity anomalies were identified, could it be distinguished from sim-

ple advection. Given the model uncertainties involved, particularly with regard to the use of mixed boundary conditions, it is suggested that this propagation mechanism should be studied in a coupled model with an improved atmosphere component—particularly one that allows the high-latitude air temperature to vary in response to SST variations. If the propagation of signals still exists, then a more detailed search for observational evidence could be made.

Much farther from the coast, *eastward* propagation of Southern Ocean SST anomalies has recently been identified in observations (with an 8–10-yr period, White and Peterson 1996), in the uncoupled LSG model (with a 45-yr timescale, Mork and Skagseth, 1996), and in a coupled O/AGCM (with a 12–16-yr timescale, Christoph et al. 1997).

5. Sensitivity to model numerics and parameterizations

The question of how sensitive the simulated variability is to a model's particular formulation can be addressed by performing the same experiment but with different OGCMs. A first attempt to do so with the Hamburg isopycnic-coordinate OGCM (OPYC: Oberhuber 1993) failed due to numerical/computational problems (Osborn 1995), but a subsequent attempt has shown variability of a similar nature (T. Barnett 1996, personal communication). The Hamburg HOPE OGCM, which is similar to the LSG OGCM except that it uses the full primitive equations, has also been integrated in a similar way and does exhibit variability of the thermohaline circulation, although the timescale is different (Drijfhout et al. 1996). A similar experiment has also been performed using the GFDL OGCM by Power (1995). He found no significant variability, although that may have been due to the weaker stochastic forcing used (Osborn 1996).

An alternative approach, used here, is to perform the same experiment repeatedly with one OGCM (the LSG model), with individual changes to the model's numerics or parameterizations. Sufficiently long integrations are necessary to assess the significance of any differences obtained. Three aspects are tested. First, the frequency with which the barotropic velocity matrix equation is re-triangularized is varied. Second, alternative convective adjustment parameterizations are used. Third, the formulation of the thermal and haline coupling of the sea ice model to the OGCM is varied.

a. Re-triangularization of the barotropic velocity matrix equation

In the LSG OGCM, the equations of motion are divided into barotropic and baroclinic components, and solved as two coupled subsystems via an implicit Euler-backward numerical scheme (Maier-Reimer et al. 1993). The barotropic subsystem is solved by direct elimination of the matrix equation, requiring two steps: matrix triangularization and back substitution. This barotropic system is described by

$$\frac{\partial u}{\partial t} - f\upsilon + \frac{g}{R\rho_0 \cos\varphi}\zeta_\lambda + \frac{1}{HR\cos\varphi}\int_{-H}^{0} p'_\lambda \, dz' = \frac{\tau^\lambda}{H\rho_0} + A_h \Delta u \tag{1a}$$

$$\frac{\partial \upsilon}{\partial t} + fu + \frac{g}{R\rho_0}\zeta_\varphi + \frac{1}{HR}\int_{-H}^{0} p'_\varphi \, dz' = \frac{\tau^\varphi}{H\rho_0} + A_h \Delta \upsilon \tag{1b}$$

$$\frac{\partial \zeta}{\partial t} - w_0 = 0, \tag{1c}$$

where u and υ are the zonal and meridional barotropic velocities, ζ is the sea surface elevation, p' is the pressure field of each baroclinic layer, τ is the wind stress, and A_h is the horizontal viscosity. Latitude is given by φ (and the meridional derivative by its subscript) and longitude by λ (and the zonal derivative by its subscript). See Maier-Reimer and Mikolajewicz (1992) for definition of the remaining symbols.

By insertion of (1c) into (1a) and (1b) a simultaneous elliptic system is obtained (not shown here). Once written in finite-difference form [see Maier-Reimer and Mikolajewicz (1992) for the resultant equations], known values of wind stress, sea surface elevation, pressure and barotropic velocity at time step t are collected on the right-hand side. This leaves only time-invariant constants multiplying the unknowns (which are u, υ, and horizontal density gradients at time step $t + 1$). The horizontal density gradients come from the fourth term on the left-hand side of Eqs. (1a) and (1b), which describe the effect of the vertically integrated pressure (due to horizontal variations in density) on the barotropic velocity. It depends upon the vertical density structure of the model and, if the basic stratification is unchanging, then this term can also be assumed to be constant in time. In that case, the matrix equation derived from (1) can be triangularized once and then solved for any right-hand side during later time steps provided that the elimination factors are retained. This is very important for the computational efficiency of the LSG model because the triangularization step is very expensive. If the density term cannot be assumed constant, then the barotropic matrix equation must be re-triangularized at every time step (or, at least, at frequent intervals).

The model's stratification changes with the phase of the thermohaline oscillations, and different sets of elimination factors are obtained if the matrix equation is triangularized at different phases. The triangularization should only be performed infrequently (making the LSG OGCM computationally very economical to integrate) if the simulated variability is insensitive to the variations

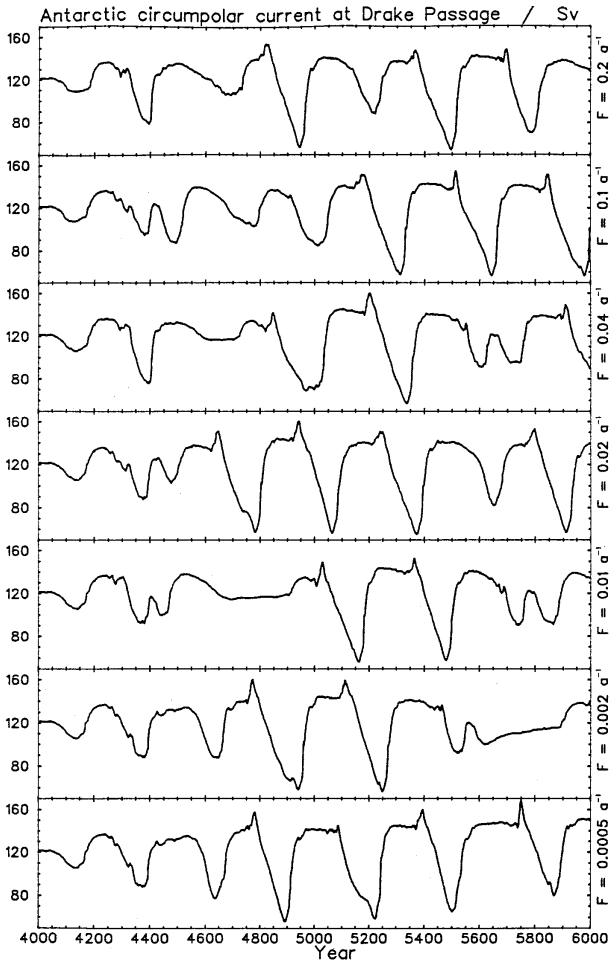

FIG. 8. Time series of ACC strength (Sv) for seven integrations with identical noise forcing, but different values of F, the frequency with which the barotropic matrix equation is re-triangularized.

in elimination factors otherwise being ignored. To test this possibility, seven 2000-yr model integrations were performed, identical except for the frequency (F) with which the triangularization was performed. In all simulations, identical sequences of spatially incoherent white noise (standard deviation 30 mm mo^{-1} everywhere) were added to the freshwater flux to excite the variability mode. The triangularization frequencies were varied from ''once every 5 years'' ($F = 0.2$ yr^{-1}) to ''once every 2000 years'' ($F = 0.0005$ yr^{-1}; that is, triangularization was performed only at the beginning of that integration).

If the ACC strength is used to compare the seven integrations (Fig. 8), it is obvious that there is no systematic dependence on F. For example, the run with $F = 0.1$ yr^{-1} is no closer to the $F = 0.2$ yr^{-1} run than are integrations with other values of F (at least in terms of the time at which the integrations begin to diverge from each other). This implies that the LSG model is behaving chaotically; the changes in the model's density field are small in just 5 yr, leading to only small differences in the elimination factors between the $F = 0.2$ yr^{-1} and the $F = 0.1$ yr^{-1} integrations, yet large differences occur in the evolution of these simulations (Fig. 8).

In case a systematic effect of F is hidden by this chaotic behavior, further analysis has been performed. A principal component analysis of key variables from each integration shows that the spatial characteristics of the variability are independent of the frequency of triangularization. Pattern correlations between the leading EOF patterns (not shown) of the seven integrations are all above 0.85 (and most are above 0.95). Analysis of the temporal characteristics of the seven integrations shows no dependence of the oscillation amplitude on F. A weak relationship was found between oscillation period and F, indicating that increasing the retriangularization frequency from 0.0005 yr^{-1} to 0.2 yr^{-1} may cause a reduction in the oscillation period from 330 to 310 years. The integrations are not, however, sufficiently long to assess the statistical significance of this relationship, and they have not been extended since it is noted that larger differences in periodicity can be introduced in other ways (Barnett et al. 1996a).

b. *Convective parameterization*

A simple parameterization of convective mixing is invoked whenever the LSG model's stratification becomes unstable. In this scheme, every adjacent pair of layers are tested for instability by comparing their potential densities (referenced to the pressure at their common interface), and the water mass properties are simply interchanged if found to be unstable. This comparison is carried out for the entire water column, beginning with the upper layers and working downward. This procedure is applied just once every time step, so the entire water column *does not necessarily become stable* throughout. It has been found experimentally that this situation arises for 5% of convecting grid-cells during a quasi-equilibrium control run (Maier-Reimer et al. 1993).

Marotzke (1991) found that the stability of the thermohaline circulation in a version of the GFDL OGCM was sensitive to the type of convective parameterization and was spontaneously unstable when a parameterization that leaves residual instabilities was used. If some residual instabilities do remain for one further time step of the GFDL model, they persist for 2 hours (or 5 days if asynchronous integration is used), whereas in the LSG model they persist for 30 days. The effect of using a different convective scheme that ensured complete stability after every time step might, therefore, be larger for the LSG model than Marotzke (1991) found.

The effects of two alternative convective schemes on the variability simulated by the LSG OGCM are presented here. The first is simply two iterations of the present scheme to remove many of the residual instabilities. The second is a switch to a scheme that *mixes* unstable water masses (as used by most other OGCMs:

Rahmstorf 1993; Oberhuber 1993) rather than interchanging them (as the present LSG scheme does).

The effect of applying, where necessary, a second iteration of the convective scheme is quite minor. Approximately 80% of the residual instabilities are removed by the second iteration, slightly raising the amount of potential energy (PE) released and intensifying the thermohaline circulation (ACC: +2.5 Sv, AABW: +1 Sv, NADW: +1 Sv). This intensification is maintained by an increase in the rate of input of PE by vertical diffusion of heat because the new convective scheme cools the deep ocean slightly (by 0.05 K) through more efficient heat release at high latitudes.

When noise forcing is applied to this new state, the model oscillates somewhat differently with the double iteration of the convective scheme (not shown) than with the old scheme. The integrations are not long enough to assess the significance of the changes, but there is an apparent tendency toward slightly weaker oscillations.

A more drastic change to the convective scheme was made next, by replacing it with one that mixes together unstable layers, rather than interchanging them (note that some numerical mixing occurred in the original LSG scheme if the unstable layers had differing thicknesses). The scheme that is used here is based on that of Rahmstorf (1993); it is computationally efficient and leaves no residual instabilities.

As the change in the parameterization of convection is much greater in this case, the freshwater flux forcing field is rediagnosed to obtain one consistent with the new parameterization. The freshwater flux used in all the mixed boundary condition simulations so far (Fig. 9a) was diagnosed from the end of a spinup integration with the old convective adjustment scheme and a restoring (i.e., relaxation) boundary condition on SSS. This process was repeated again, but with the spinup integration performed using the new mixing convective scheme. The differences between the newly diagnosed freshwater flux forcing and the original forcing (Fig. 9b) are, as expected, in the regions of convective activity. The largest change is in the Amundsen sector, where the net input of freshwater (Fig. 9a) is considerably enhanced (Fig. 9b). This is because near-surface vertical salinity and temperature gradients are much stronger in that sector.

From the end of the new spinup integration (with restoring boundary conditions), the model with the mixing convective scheme was integrated under mixed boundary conditions for 4000 yr. During this period it was forced by the newly diagnosed freshwater flux field (Fig. 9b) and, during the second 2000 yr only, white noise was added to the freshwater flux (with a uniform standard deviation of 30 mm mo^{-1}). The model shows an initial adjustment to the switch to mixed boundary conditions (Fig. 10d) and then maintains a quasi-stable state until the stochastic forcing is begun (year 10 000). It then begins to show some low-frequency variability with a timescale of around 600 yr. As a comparison, a similar 4000-yr simulation (stochastic forcing again applied only to the second half) with the standard convection scheme and the standard FWF forcing is shown in Fig. 10a. Comparison of the simulations indicates that the new convection scheme combined with the new forcing produces greater high-frequency noise (Fig. 10d, cf. Fig. 10a), but that the stochastic-forcing-induced low-frequency variability is considerably weaker (in fact, the standard deviation of these low-frequency variations in the ACC strength is only 5.5 Sv, compared to 20.6 Sv for Fig. 10a).

The reduced low-frequency variability is due mainly to the newly diagnosed freshwater flux forcing field, with less contribution coming from the change in convective scheme. To illustrate this, similar simulations have been performed using the standard, interchange convective scheme forced by the newly diagnosed FWF (Fig. 10b) and using the new, mixing convective scheme forced by the standard FWF (Fig. 10c). The *interchange* scheme shows some adjustment to the new forcing field (Fig. 10b), resulting in an increase in ACC strength over the first 2000 yr. When stochastic forcing is begun, only relatively weak low-frequency variability is generated (although with a shorter periodicity than is obtained using the mixing scheme). The *mixing* scheme results in spontaneous oscillations occurring (i.e., without the need for stochastic forcing) when the standard freshwater flux forcing field is used (Fig. 10c). Such spontaneous oscillation is not unique to the mixing convective scheme since the interchange scheme can also result in spontaneous oscillations under some conditions (see PBM95). When stochastic forcing is begun (Fig. 10c), the simulation is very similar to that obtained with the standard scheme (Fig. 10a) in timescale and magnitude.

To test the robustness of the effect of the newly diagnosed freshwater flux field on the magnitude of the internal variability, integrations with much stronger FWF stochastic forcing (std dev 150 mm mo^{-1}) were performed (Fig. 11) for the two cases that failed to generate strong variability (Figs. 10b and 10d). Both integrations, with the new FWF field diagnosed to be consistent with the mixing convective scheme, oscillate more strongly with the stronger noise forcing, but still only one-half as strong as with the standard FWF field, whether the interchange (Fig. 11a) or the mixing (Fig. 11b) convective scheme is used.

Finally, note that only the simulations shown in Figs. 10a, 10d, and 11b use freshwater flux fields consistent with the model version being used. The mismatch between forcing fluxes and model fluxes in the other cases leads to a small drift in the model's state. This drift, while small, is generally such that the error between simulated and observed (Levitus 1982) surface salinity worsens in the annual mean. It could be argued, therefore, that the dramatic reduction in low-frequency variability between Figs. 10a and 10d *is* due to the change in convection scheme, but only because the new scheme implies a different field of surface freshwater fluxes. These uncertainties can only be reduced by additional observational constraints on the true precipitation and evaporation fields.

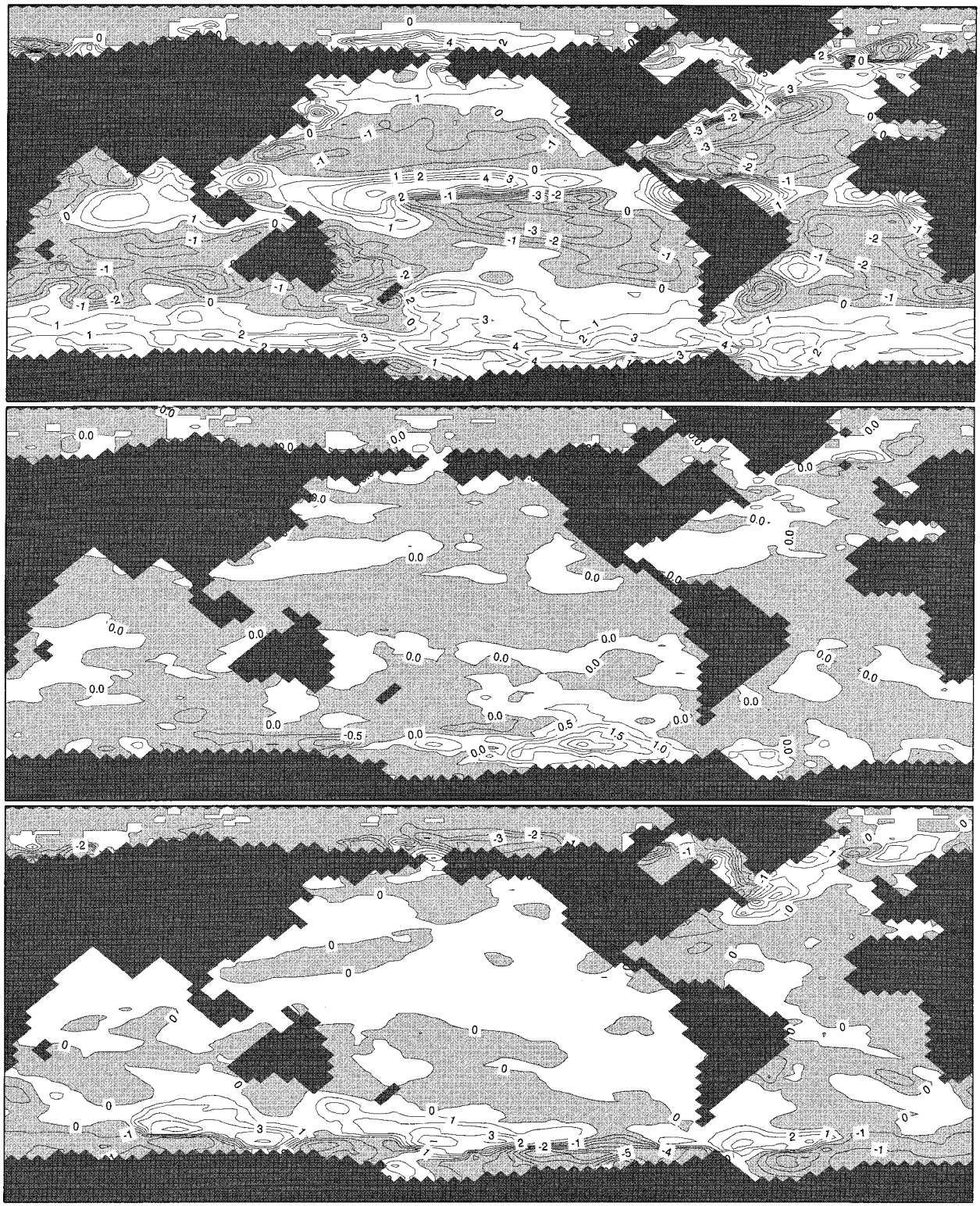

FIG. 9. Annual-mean net surface freshwater flux (mm day^{-1}) diagnosed from a control run under relaxation boundary conditions. (a) For the standard LSG model, (b) difference between the field diagnosed with the mixing convective scheme and (a), and (c) difference between the field diagnosed with the new ice–ocean coupling and (a).

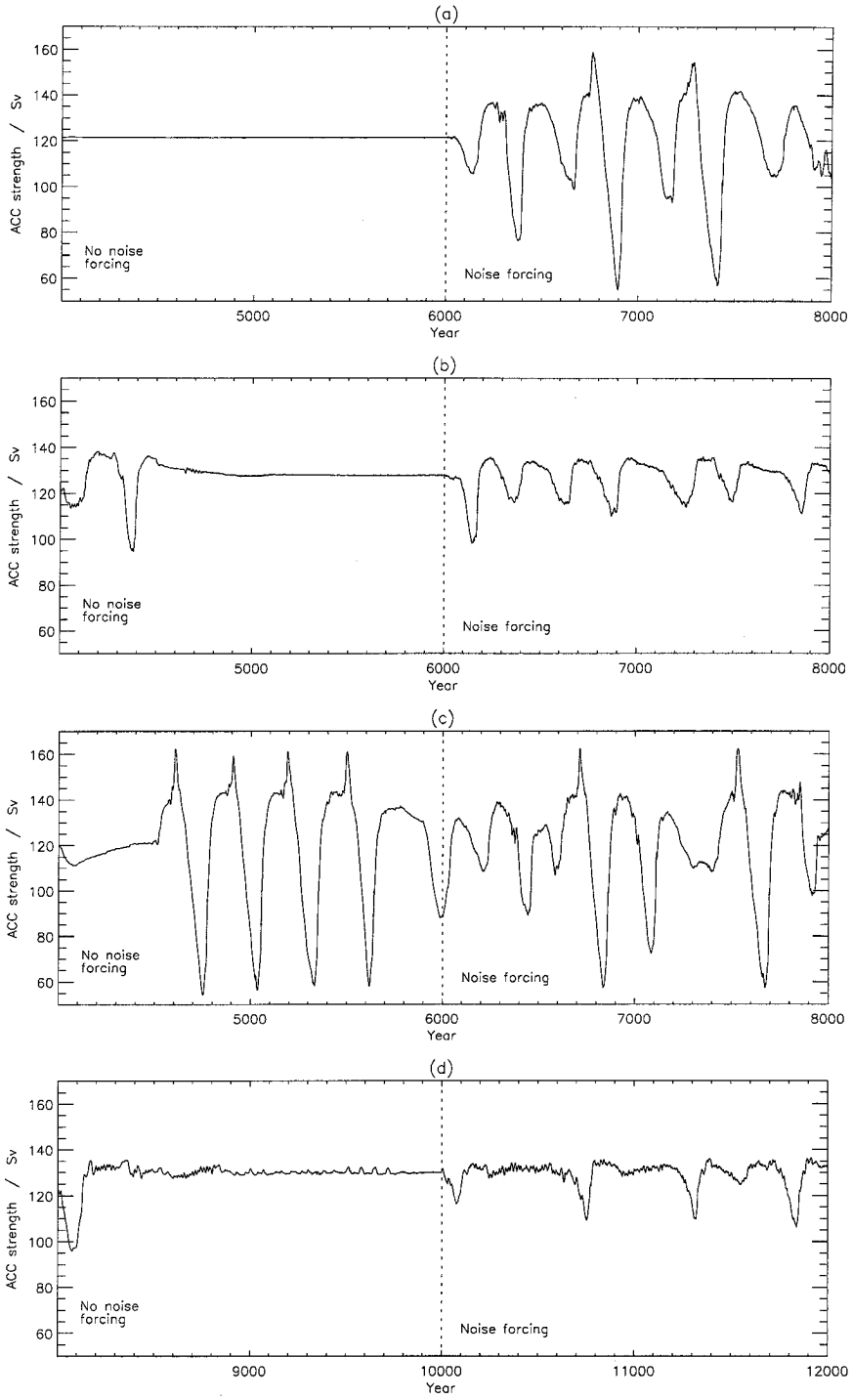

FIG. 10. ACC strength (Sv) from four integrations under mixed boundary conditions, with noise forcing only in the second 2000 yr of each simulation. Standard LSG model used in (a) and (b). LSG model with mixing convective scheme used in (c) and (d). Standard freshwater flux used in (a) and (c). Newly diagnosed freshwater flux used in (b) and (d).

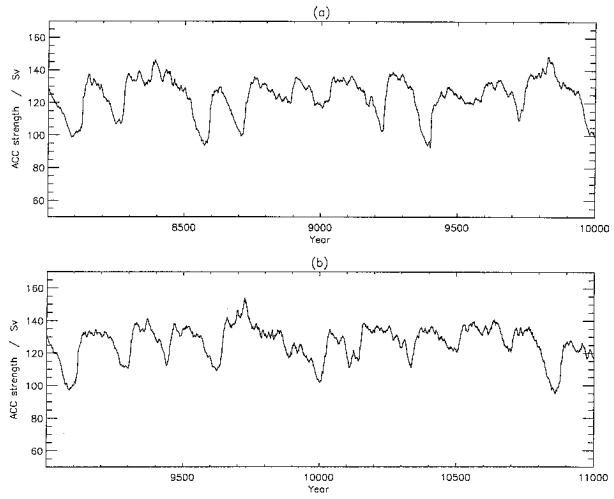

FIG. 11. ACC strength (Sv) from two integrations under mixed boundary conditions with very strong noise forcing, and the newly diagnosed freshwater flux. Standard LSG model used in (a). LSG model with mixing convective scheme used in (b).

c. Sea ice parameterization

In section 4b, it was identified that the sea ice component of the LSG model performs in an unrealistic way. When sea ice forms, instead of transferring some of the very saline brine that is generated downward into the second model layer down, salt is in fact transferred from layer two upward into the uppermost model layer. An upward salt flux occurs between the upper two model layers throughout the Antarctic sea ice cover region.

The algorithm used in the LSG OGCM to determine the thermal and haline coupling between ice and ocean is the cause of this unexpected flux. When sea ice is present, convection between the upper two layers is prevented by ensuring that they are always stable or neutrally stable. Additional vertical mixing is employed in the sea ice scheme to ensure this stability, and it is this mixing that causes the strong upward salt (and heat) flux. The temperatures of the water of the top two layers are mixed whenever sea ice is present. If sea ice is melting, the freshwater released is added to the upper layer only; if sea ice is forming, the salt released is also added to the upper layer only—but then the salinities of the top two layers are mixed. This mixing obtains the stability required: the upper layer will have the same temperature and the same, or lower, salinity as the layer below.

This is different than *rejecting* salt into the second layer down since this scheme involves the existing salinity of the second layer. If the initial salinity of the second layer is greater than that of the upper layer (even after augmentation by the brine from ice formation), then the mixing will yield an upward flux. This occurs throughout the Antarctic sea ice covered region in the annual mean—and even for over 90% of individual monthly time steps. For this to continue throughout the integration, the second layer must be gaining salt from the (warm) saline water moving poleward at depth.

The heat budget is affected too. The mixing of the temperatures of the upper two layers (each 50 m thick) in the presence of sea ice results in an effective mixed layer of 100 m, even if the layers are stratified. This relatively thick mixed layer will probably reduce the volume of sea ice formed. The air–sea heat flux will also be somewhat enhanced, due to the heat flux from the second layer into the uppermost layer. A heat budget for the surface of the Weddell sector (not shown) indicates that this area-averaged flux exceeds 60 W m^{-2} in the annual mean at times and is larger than the convective, advective, and diffusive fluxes.

An alternative scheme for the thermal and haline coupling between sea ice and ocean has been implemented. When sea ice forms, the brine is rejected into the upper two layers in equal quantities. When sea ice melts, the freshwater is input into the upper layer, as in the present scheme. The uppermost two layers are no longer automatically mixed, but the convection scheme is altered so that convection is correctly dealt with between the upper two layers even when sea ice is present. The interchange scheme is used rather than the mixing scheme implemented in the previous section, and two iterations are used to remove most residual instabilities.

A new freshwater flux forcing field is then diagnosed from the final 50 yr of an 8000 yr integration with the new model (with relaxation conditions on both SST and SSS). The annual-mean difference between this new forcing field and the standard LSG forcing is shown in Fig. 9c. In the sea ice covered areas of the Southern Ocean, the net input of freshwater has been very much reduced because a large input of freshwater is no longer required to offset the upward flux of salt induced by the old ice–ocean coupling. In the sector means, which extend past the ice edge, this change is largely offset by an increase in the FWF input immediately to the north of the ice edge. Changes in the North Atlantic Ocean are more complex with smaller-scale structures.

Air–sea freshwater and heat fluxes are not well observed in the high latitudes of the Southern Ocean, so it is not certain whether the effect of the present LSG ice–ocean coupling on surface fluxes is detrimental. It is of interest to note, however, that the freshwater and heat fluxes that the ECHAM1 AGCM predicts in the Southern Ocean are somewhat different from those that the LSG OGCM requires (Gates et al. 1993, their Figs. 7 and 6 respectively), thereby requiring a flux adjustment to be made when the models are coupled. The sign of these adjustments are such that the new FWF field (Fig. 9c) would reduce the magnitude of the adjustment needed in the southern Ross and Amundsen sectors (which is where the largest flux adjustments were needed). The increases in FWF that occur to the north of the ice edge would, however, increase the flux adjustment required there.

The new coupling also results in a different pattern

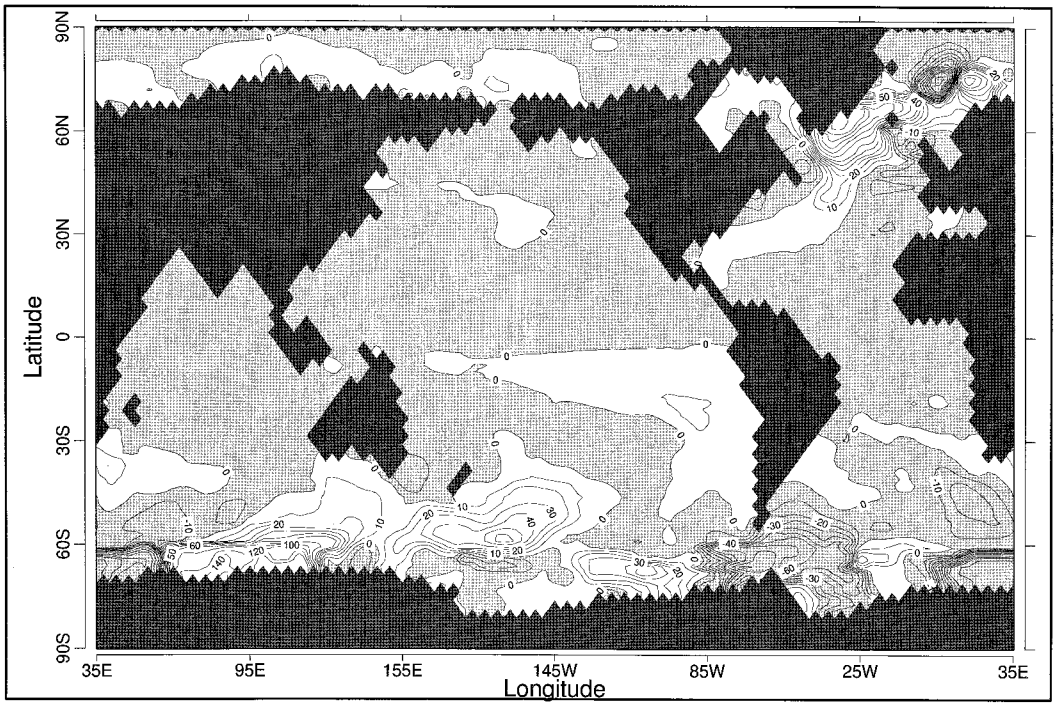

FIG. 12. Annual-mean net heat flux difference (W m^{-2}) between the case with the new ice–ocean coupling and the standard LSG case.

of air–sea heat flux (see Fig. 12 for the pattern of change between the new coupling case and the standard case). The changes are very large in the convectively active regions, although the pattern can vary from year to year due to the sporadic nature of convection. In the Southern Ocean, there are increases in oceanic heat loss in the Drake Passage and parts of the Weddell and Enderby sectors, and decreases elsewhere. The ECHAM1 AGCM does not require/compute as large heat fluxes out of the ocean as the LSG OGCM requires over the eastern Enderby, northern Ross and Wilkes sectors, and over the Weddell Sea (Gates et al. 1993, their Fig. 6). The changes introduced by the new ice–ocean coupling appear to bring the OGCM fluxes (Fig. 12) closer to the AGCM fluxes in the Enderby, Ross, and Wilkes sectors (perhaps reducing the magnitude of the required flux adjustment), but would worsen the mismatch in the Weddell Sea. The reduction of heat loss from the northern North Atlantic would also reduce the heat flux adjustment required when coupling the two models (Gates et al. 1993, their Fig. 6).

With the new ice–ocean coupling and the new freshwater flux forcing field, the LSG OGCM was integrated under mixed boundary conditions for 4000 yr (beginning from the end of the simulation with a restoring boundary condition on SSS from which the FWF forcing was rediagnosed). Stochastic forcing was applied to the second 2000 yr only (white noise with a standard deviation of 30 mm mo^{-1} once more). *Very little variability occurs,* even when stochastically forced, as shown by the ACC strength (Fig. 13a). This transport strengthens considerably at first and then maintains a very steady strength of 150 Sv (Sv $\equiv 10^6$ m^3 s^{-1}), until noise forcing is begun. The noise forcing triggers a reduction in ACC strength to 130 Sv and then shows only small variations (<5 Sv) for the subsequent 1800 yr. It appears that the model changes from one state to another rapidly (as shown by the formation rate of Antarctic Bottom Water, Fig. 13b) and the ACC responds slowly to these switches on a 50 to 100 yr timescale. The AABW formation rate shows sudden changes between values of 25, 1, 20, 10, and 20 Sv during the first 2000 yr, and then to 10, 1, 10, and 5 Sv during the second 2000 yr with noise forcing.

Although there is much reduced variability in the Southern and Atlantic Oceans in this simulation, there is now some variability in the convective activity of the upper North Pacific Ocean (Fig. 14c). Oscillations with a period of 40 yr were identified in the upper 250 m of the entire Bering Sea.

Surface salinity and heat budgets (not shown) for the Weddell sector confirm that the new coupling produces more realistic fluxes associated with the sea ice. The old coupling formulation caused a mean salinification of the surface of 0.25 psu yr^{-1} (Fig. 5d), whereas the new coupling causes a freshening of 0.24 psu yr^{-1} (by transporting salt down into the second layer). This has not led to a lower sector-mean input of freshwater at the surface since the salinity tendency due to convection has increased greatly. The latter increase is due to an

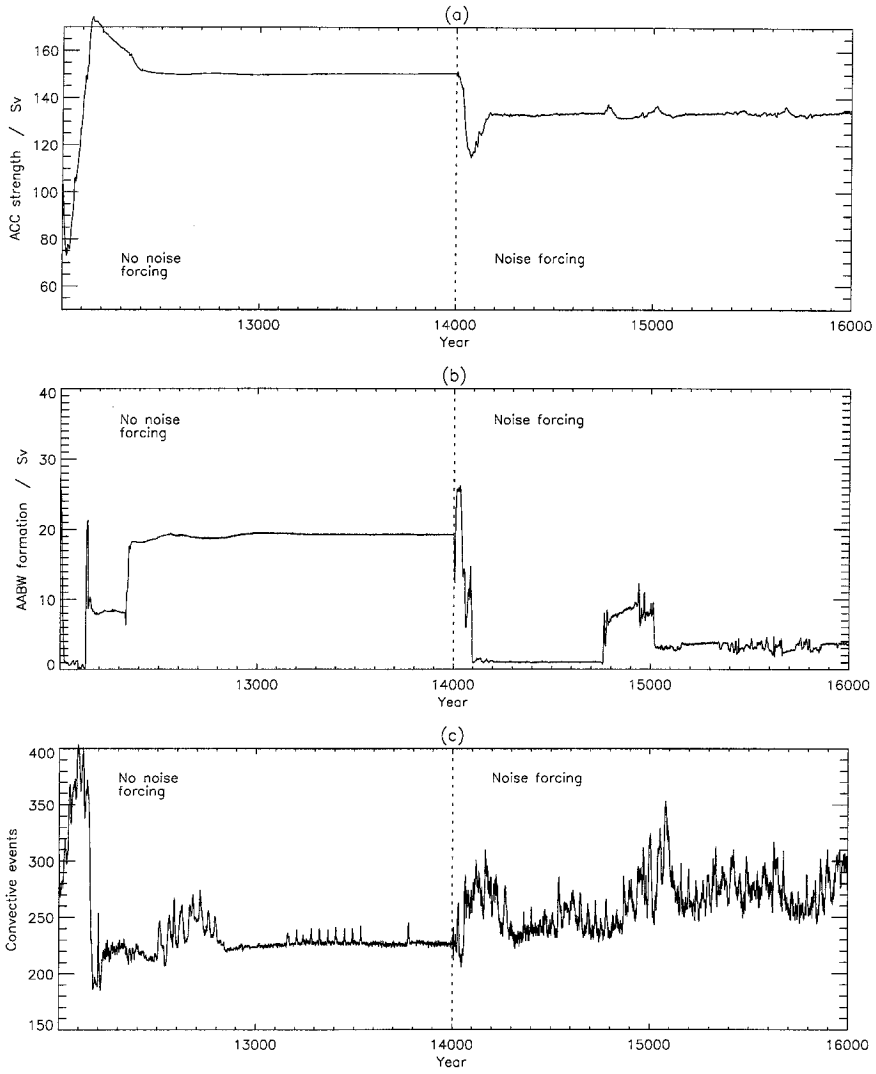

FIG. 13. (a) ACC strength (Sv); (b) AABW formation rate (Sv); (c) number of convective events at 200-m depth in January. From the simulation with the new ice–ocean coupling, under mixed boundary conditions, with noise forcing only in the second 2000 yr of the simulation.

increase in convective events and an increase in the salinity gradient between the upper two layers. [As we have seen, the input of freshwater in just the sea-ice-affected areas *does* decrease considerably (Fig. 9c).]

The old coupling formulation resulted in a mean heat flux from layer 2 to layer 1 of 50 W m^{-2} in the Weddell sector due to *mixing* of these layers whenever sea ice was present. The new scheme removes this automatic mixing, allowing convective interchange only if they are statically unstable. There is now no heat flux due to the sea ice forcing (except from its modification of the air–sea fluxes), but this has led to only a small reduction in sector-mean air–sea heat loss since it too is partly offset by an increase in the convective heat flux into the uppermost layer (which has doubled from 40 to 80 W m^{-2}).

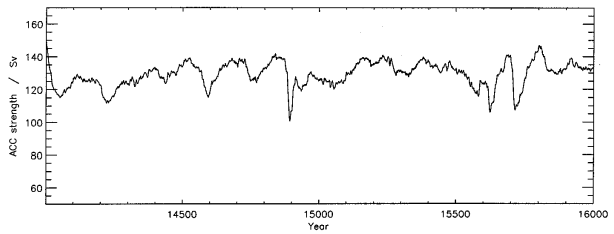

FIG. 14. ACC strength (Sv) from an integration with the new ice–ocean coupling and very strong freshwater flux noise forcing.

To further test the robustness of the apparent reduction in variability that the new ice–ocean coupling causes, a very high level of stochastic forcing (standard deviation 150 mm mo^{-1}) was added to the freshwater flux everywhere. In this integration, there is now more variability of the ACC strength (Fig. 14), although the

TABLE 1. Number of grid-box columns with convective potential energy release of at least 2 mW m^{-2} and the percentage of these that have a net surface freshwater flux (FWF) (positive into the ocean) in the given ranges. Results from the standard LSG OGCM and from the version with the improved ice–ocean coupling. Figures in parentheses are for the Southern Hemisphere only.

	Standard LSG	New ice–ocean coupling
FWF range (mm day^{-1})	Number of convecting columns 307 (236)	272 (182)
−10 to −1	9.4% (3.8%)	15.1% (9.9%)
−1 to +1	24.8% (26.7%)	30.1% (35.2%)
+1 to +10	65.8% (69.5%)	54.4% (54.9%)

magnitude remains considerably weaker than that obtained with the old coupling (e.g., Fig. 8). The variability occurs over a range of timescales, with a broad, but weak, spectral peak at 140 yr. The variability is associated with changes in Southern Ocean convective activity and AABW formation rate, but dramatic amplification of surface salinity anomalies does not occur; convection is never completely suppressed by a freshwater cap.

The much reduced levels of variability are due, in part at least, to the changes in the freshwater flux forcing that the new scheme requires. [These changes may be in the correct direction to reduce the flux correction required when coupling the LSG OGCM to an atmosphere model (but that cannot be confirmed without performing an identical spinup procedure to that used in previous coupling attempts), which is an indication that the new ice–ocean coupling may be an improvement. The paucity of observed freshwater fluxes over the Southern Ocean leaves considerable uncertainty.] There is not an overall decrease in net freshwater flux input to the ocean, but there is a shift northward in the maximum input (Fig. 9c). This shift moves the maximum input away from the most convectively active locations (which are near or under the ice cover in the LSG model's Southern Ocean). There is a reduction in the number of convecting water columns in the LSG OGCM when the new coupling is used, but more importantly the convectively active water columns are now more frequently located in areas with little freshwater input or net freshwater removal (Table 1). With the standard LSG ice–ocean coupling, the proportion of convectively active water columns located in regions where the net input of freshwater was greater than 1 mm day^{-1} was 10% higher. The difference is 15% if the Southern Hemisphere is considered alone (Table 1). As discussed in detail in section 2, the convective feedback is strongest where convection occurs in a region of strong freshwater input. The changes brought about by the new coupling weaken the convective feedback and thereby weaken the model's internally generated variability.

6. Summary and conclusions

New experiments and their results have been described that investigate further the internally generated variability previously identified in the Hamburg LSG ocean general circulation model. These results augment and extend the earlier work of MM90 and PBM95, who studied oscillations that occur with a periodicity of 320 years when the OGCM is integrated under mixed boundary conditions. The convective feedback (Power 1995; Drijfhout et al. 1996) is one of the key processes in the generation of these oscillations and it operates in regions of convective activity that have a net input of freshwater at the surface. To operate, it requires the strong constraint upon surface temperature variations relative to surface salinity variations that mixed boundary conditions provide.

Mikolajewicz and Maier-Reimer (1990) identified the propagation of salinity anomalies around the Atlantic thermohaline circulation in the meridional–vertical plane. In the present study, it has been shown that these are merely signals emitted from the source of the variability in the Southern Ocean; they do not appear to play an active role in the generation of the oscillations. The Southern Ocean flip–flop oscillator of Pierce et al. (1995) is, therefore, the mechanism that generates the variability.

A second mode of signal propagation has been identified that provides a link between the timing of the thermohaline oscillations at each longitude of the Southern Ocean and that may play some role in determining the periodicity of the internal variability. Salinity anomalies move westward around the Antarctic coast. The mechanism for this propagation (that is against the direction of the flow field at most longitudes) is a coastally trapped wave, driven by coupled variations in upper-ocean density and coastal upwelling and maintained by the convective feedback. The same mechanism operates in the Hamburg HOPE model (Drijfhout et al. 1996).

In addition to the identification and analysis of anomaly propagation, sensitivity studies have been done to investigate the effects of uncertainties in some of the model's numerics and physics. It was shown that the frequency with which the matrix equation of the barotropic velocity component is re-triangularized is only of little importance to the characteristics of the simulated variability. This is, computationally, a very expensive step of the model integration, so it is beneficial that this study has shown that it can be performed quite infrequently without adversely affecting the model results. The precise evolution of an integration is, however, dependent on the frequency with which the matrix is re-triangularized since the model rapidly amplifies the small differences introduced into the elimination factors (these factors are stored for use in all subsequent time steps).

Convective adjustment is parameterized very simply in most ocean models, and the degree of realism of the various algorithms is unclear. Should statically unstable water masses be mixed together or interchanged? Should the entire instability be removed within one

model time step? The aim of the present study was not to answer these questions, but to ascertain whether the model simulation is sensitive to the choice of algorithm. These uncertainties are only critical if the model is sensitive to the parameterization used.

The standard LSG model uses a convective scheme that interchanges water masses but does not guarantee complete stability. Removing some of the residual instabilities, via a second application of the same scheme, has a small effect on the characteristics of the simulated variability, possibly causing a small reduction in the amplitude and period of the Southern Ocean oscillations. Using an algorithm that mixes rather than interchanges, unstable water masses has a greater impact—provided that a new freshwater flux forcing field is diagnosed that is consistent with the new algorithm. The peak-to-peak amplitude of the variability is reduced from 100 to 30 Sv. The decrease is attributed almost entirely to the new freshwater flux forcing.

Most OGCMs that include the effects of brine rejection due to sea ice formation do so by parameterizing it as a rejection into subsurface layers. It was shown that the LSG OGCM behaves rather differently and probably unrealistically: the effect of its sea ice algorithm is to transfer salt upward from the second layer to the surface layer. Implications of this for heat fluxes, surface fluxes, and convection were considered too. Replacing the existing thermal and haline coupling between ice and ocean components with a more realistic one resulted in a quite different surface flux forcing and a quite different model behavior. The variability was greatly reduced, and neither weak nor strong stochastic forcing was able to generate strong Southern Ocean oscillations. The changed surface fluxes are the cause of this reduction: convectively active water columns are more frequently located in areas with little freshwater input or even net freshwater removal than with the old ice–ocean coupling. Hence, the convective feedback can operate on fewer water columns.

The problems with the old ice–ocean coupling are also relevant to studies that have coupled the LSG OGCM to an atmosphere GCM. There is some similarity between the patterns of flux adjustments required in such coupled atmosphere–ocean models (e.g., see Gates et al. 1993) and the change in flux fields implied by the new ice–ocean coupling developed here. In particular, with the new ice–ocean coupling the LSG OGCM requires less input of freshwater and less removal of heat from parts of the high-latitude Southern Ocean—changes that might decrease the flux adjustment required when coupling the model to the ECHAM1 AGCM. Changes in other regions may be detrimental, but specific tuning of the OGCM while using the new ice–ocean coupling might ameliorate these.

The variability of the LSG OGCM is very sensitive to the freshwater flux forcing used. This is true of other ocean models too. While the sensitivity is reduced when mixed boundary conditions are not used, it is still undesirable to force an ocean model with a FWF diagnosed from an integration of the model itself: it may hide systematic model errors in the steady-state simulation, but to the detriment of the model's simulation of variability. Improved observations of all freshwater flux terms are required, seasonally and globally. Even if such forcing fields were available, current ocean models may be unable to simulate a realistic steady state when forced by them; in that case, improvements to the models would also be required.

The sensitivity studies described here do not cover all possibilities; it is important to know whether the same internally generated variability occurs if the horizontal or vertical resolution were changed, if more realistic sea–ice dynamics were modeled or if marginal sea and slope convection were parameterized.

In view of the detailed discussion presented in section 2, it is clear that air temperature should be allowed to vary in response to ocean changes since the convective feedback is unrealistically strong if air temperature is held fixed. That is a disadvantage of the mixed boundary conditions used here, and the simulated variability would be weaker if they were improved upon. It is even possible that this type of variability would not occur at all; in that case, the sensitivity studies described here are still relevant, but as an extremely sensitive test case. See section 2 for references to work that considers the effect of allowing air temperature to vary in response to ocean changes.

Acknowledgments. This research was supported by the U.S. Dept. of Energy (DE-FG02-86ER60397 and DE-FG03-91ER61215). The Climate Impacts LINK Project (U.K. Dept. of Environment EPG/1/1/16) provided computing facilities for some of the model integrations. Tim Barnett and Tom Wigley are thanked for their support of this work; discussion with David Pierce was extremely valuable; the comments of two anonymous reviewers helped me to clarify parts of this paper; and Uwe Mikolajewicz generously made the LSG OGCM available for this work.

REFERENCES

Barnett, T. P., M. Chu, R. Wilde, and U. Mikolajewicz, 1996a: Low frequency ocean variability induced by stochastic forcing of various colors. *Proc. National Research Council Workshop on Decade-to-Century Time Scales of Climate Variability*, Irvine, CA, 398–405.

——, B. D. Santer, P. D. Jones, R. S. Bradley, and K. R. Briffa, 1996b: Estimates of the low frequency natural variability in near surface air temperature. *The Holocene*, **6,** 255–263.

Christoph, M., T. P. Barnett, and E. Roeckner, 1997: The Antarctic Circumpolar Wave in a coupled ocean–atmosphere GCM. MPI Rep. 235, 28 pp. [Available from Max-Planck Institute for Meteorology, Bundesstrasse 55, Hamburg 20146, Germany.].

Delworth, T., S. Manabe, and R. J. Stouffer, 1993: Interdecadal variability of the thermohaline circulation in a coupled ocean–atmosphere model. *J. Climate*, **6,** 1993–2011.

Drijfhout, S., C. Heinze, M. Latif, and E. Maier-Reimer, 1996: Mean

circulation and internal variability in an ocean primitive equation model. *J. Phys. Oceanogr.,* **26,** 559–580.
Gates, W. L., U. Cubasch, G. A. Meehl, J. F. B. Mitchell, and R. J. Stouffer, 1993: An intercomparison of selected features of the control climates simulated by coupled ocean–atmosphere general circulation models. SGGCM, WCRP-82, WMO TD 574. [Available from World Meteorological Organization, Case Postale 2300, CH-1211 Geneva 2, Switzerland.]
Haney, R. L., 1971: Surface thermal boundary conditions for ocean circulation models. *J. Phys. Oceanogr.,* **1,** 241–248.
Hellermann, S., and M. Rosenstein, 1983: Normal monthly wind stress over the world ocean with error estimates. *J. Phys. Oceanogr.,* **13,** 1093–1104.
Jones, P. D., 1989: Influence of ENSO on global temperatures. *Climate Mon.,* **17,** 80–89.
Kushnir, Y., 1994: Interdecadal variations in North Atlantic sea surface temperature and associated atmospheric conditions. *J. Climate,* **7,** 141–157.
Lemke, P., E. W. Trinkl, and K. Hasselmann, 1980: Stochastic dynamic analysis of polar sea-ice variability. *J. Phys. Oceanogr.,* **10,** 2100–2120.
Levitus, S., 1982: *Climatological Atlas of the World Ocean.* NOAA Prof. Paper No. 13, U.S. Govt. Printing Office, 173 pp.
Lunkeit, F., R. Sausen, and J. M. Oberhuber, 1996: Climate simulations with the global coupled atmosphere–ocean model ECHAM2/OPYC, Part I: Present-day climate and ENSO events. *Climate Dyn.,* **12,** 195–212.
Maier-Reimer, E., and U. Mikolajewicz, 1992: The Hamburg large-scale geostrophic ocean general circulation model (cycle 1). DKRZ Tech. Rep. 2, 34 pp. [Available from Max-Planck Institute for Meteorology, Bundesstrasse 55, Hamburg 20146, Germany.]
——, ——, and K. Hasselmann, 1993: Mean circulation of the Hamburg LSG OGCM and its sensitivity to the thermohaline forcing. *J. Phys. Oceanogr.,* **23,** 731–757.
Manabe, S., and R. J. Stouffer, 1988: Two stable equilibria of a coupled ocean–atmosphere model. *J. Climate,* **1,** 841–866.
Marotzke, J., 1991: Influence of convective adjustment on the stability of the thermohaline circulation. *J. Phys. Oceanogr.,* **21,** 903–907.
Mikolajewicz, U., and E. Maier-Reimer, 1990: Internal secular variability in an ocean general circulation model. *Climate Dyn.,* **4,** 145–156.
——, and ——, 1994: Mixed boundary conditions in ocean general circulation models and their influence on the stability of the model's conveyor belt. *J. Geophys. Res.,* **99,** 22 633–22 644.
Mitchell, J. F. B., R. A. Davis, W. J. Ingram, and C. A. Senior, 1995: On surface temperature, greenhouse gases, and aerosols: Models and observations. *J. Climate,* **8,** 2364–2386.
Mork, K. A., and O. Skagseth, 1996: Modelling the ocean response to secular surface temperature transitions. *Climate Dyn.,* **12,** 653–666.
Oberhuber, J. M., 1988: An atlas based on the COADS dataset: The budgets of heat, buoyancy and turbulent kinetic energy at the surface of the global ocean. MPI Rep. 15, 20 pp. [Available from Max-Planck Institute for Meteorology, Bundesstrasse 55, Hamburg 20146, Germany.]
——, 1993: Simulation of the Atlantic circulation with a coupled sea-ice–mixed layer–isopycnal general circulation model. Part I: Model description. *J. Phys. Oceanogr.,* **23,** 808–829.
Osborn, T. J., 1995: Internally-generated variability in some ocean models on decadal to millennial timescales. Ph.D. thesis, University of East Anglia, Norwich, United Kingdom, 650 pp.
——, 1996: Comment on ''Climate drift in a global ocean general circulation model.'' *J. Phys. Oceanogr.,* **26,** 1661–1663.
Pierce, D. W., T. P. Barnett, and U. Mikolajewicz, 1995: Competing roles of heat and freshwater flux in forcing thermohaline oscillations. *J. Phys. Oceanogr.,* **25,** 2046–2064.
——, K.-Y. Kim, and T. P. Barnett, 1996: Variability of the thermohaline circulation in an ocean general circulation model coupled to an atmospheric energy balance model. *J. Phys. Oceanogr.,* **26,** 725–738.
Power, S. B., 1995: Climate drift in a global ocean general circulation model. *J. Phys. Oceanogr.,* **25,** 1025–1036.
——, and R. Kleeman, 1994: Surface heat flux parameterisation and the response of OGCMs to high-latitude freshening. *Tellus,* **46A,** 86–95.
Rahmstorf, S., 1993: A fast and complete convection scheme for ocean models. *Ocean Modelling* (unpublished manuscript), **101,** 9–11.
——, 1995: Bifurcations of the Atlantic thermohaline circulation in response to changes in the hydrological cycle. *Nature,* **378,** 145–149.
——, and J. Willebrand, 1995: The role of temperature feedback in stabilizing the thermohaline circulation. *J. Phys. Oceanogr.,* **25,** 787–805.
Santer, B. D., K. E. Taylor, T. M. L. Wigley, P. D. Jones, D. J. Karoly, J. F. B. Mitchell, A. H. Oort, J. E. Penner, V. Ramaswamy, M. D. Schwarzkopf, R. J. Stouffer, and S. F. B. Tett, 1996: A search for human influences on the thermal structure of the atmosphere. *Nature,* **382,** 39–46.
Schlesinger, M. E., and N. Ramankutty, 1994: An oscillation in the global climate system of period 65–70 years. *Nature,* **367,** 723–726.
Schneider, E. K., and J. L. Kinter III, 1994: An examination of internally generated variability in long climate simulations. *Climate Dyn.,* **10,** 181–204.
Seager, R., Y. Kushnir, and M. A. Cane, 1995: A note on heat flux boundary conditions for ocean models. *J. Phys. Oceanogr.,* **25,** 3219–3230.
Stocker, T. F., and L. A. Mysak, 1992: Climatic fluctuations on the century timescale: A review of high-resolution proxy data and possible mechanisms. *Clim. Change,* **20,** 227–250.
Stommel, H., 1961: Thermohaline convection with two stable regimes of flow. *Tellus,* **13,** 224–230.
Stouffer, R. J., S. Manabe, and K. Y. Vinnikov, 1994: Model assessment of the role of natural variability in recent global warming. *Nature,* **367,** 634–636.
Trenberth, K. E., 1990: Recent observed interdecadal climate changes in the Northern Hemisphere. *Bull. Amer. Meteor. Soc.,* **71,** 988–993.
von Storch, J.-S., 1994: Interdecadal variability in a global coupled model. *Tellus,* **46A,** 419–432.
Welander, P., 1982: A simple heat-salt oscillator. *Dyn. Atmos. Ocean.,* **6,** 233–242.
White, W. B., and R. G. Peterson, 1996: An Antarctic Circumpolar Wave in surface pressure, wind, temperature and sea-ice extent. *Nature,* **380,** 699–702.
Wigley, T. M. L., and S. C. B. Raper, 1990: Natural variability of the climate system and detection of the greenhouse effect. *Nature,* **344,** 324–327.
——, and ——, 1991: Detection of the enhanced greenhouse effect on climate. *Climate Change: Science, Impacts and Policy,* J. Jager, Ed., Cambridge University Press, 231–242.
Woodruff, S. D., R. J. Slutz, R. L. Jenne, and P. M. Steurer, 1987: A comprehensive ocean–atmosphere dataset. *Bull. Amer. Meteor. Soc.,* **68,** 1239–1250.
Zhang, S., R. J. Greatbatch, and C. A. Lin, 1993: A reexamination of the polar halocline catastrophe and implications for coupled ocean–atmosphere modeling. *J. Phys. Oceanogr.,* **23,** 287–299.